Drone Imagery Applied to Enhance Flood Modeling

Brianna Friedman

Thesis submitted to the faculty of the Virginia Polytechnic Institute and State University in partial fulfillment of the requirements for the degree of

Master of Science

in

Mechanical Engineering

Kevin B. Kochersberger, Chair

Venkataramana R. Sridhar

Michael J. Roan

May 5, 2021

Blacksburg, Virginia

Keywords: Flood Modeling, Drone Imagery, Data-Scarce, Low-Resource

Drone Imagery Applied to Enhance Flood Modeling

Brianna Friedman

ABSTRACT

Accessible flood modeling for low-resource, data-scarce communities currently does not exist. This paper proposes using drone imagery to compensate for the lack of other flood modeling data (i.e. streamflow measurements). Three flood models were run for Dzaleka Refugee Camp, located in Dowa, Malawi. Two of the models (the Soil & Water Assessment Tool (SWAT) and the Hydrologic Engineering Center River Analysis System (HEC-RAS)) are commonly used hydrological-hydraulic based models. The third model, the Water Caused Erosion Patterns (WCEP) model, was proposed by the author to capitalize on the high-resolution drone imagery using geological-geomorphological information. The drone imagery used in this study has a resolution of 3.5cm and shows erosion patterns throughout the refugee camp. By comparing the erosion patterns to flow direction of the surface, the erosion patterns were determined to be water caused or not water caused, the erosion patterns considered water caused were defined as high-risk flood areas, creating the WCEP model.

The three models were compared using locations of collapsed houses throughout the camp. It was found that the WCEP model represents the location of collapsed houses significantly better (misclassification rate below 17%) than the SWAT or HEC-RAS models (misclassification rate below 54%, and 67% respectively). The WCEP model was

combined with the best hydrological-hydraulic model (SWAT) to create a hydrogeomorphological model which capitalizes on both the drone imagery and the hydrological process.

Drone Imagery Applied to Enhance Flood Modeling

Brianna Friedman

GENERAL AUDIENCE ABSTRACT

The negative impact flooding has on communities can be reduced through flood modeling. But commonly used flood models are not accessible to data-scarce communities because of the historical data the models require. This paper explores using aerial imagery taken by a drone to make-up for the lack of historical data at Dzaleka Refugee Camp located in Dowa, Malawi.

Drone imagery has a very high spatial resolution (3.5cm), so it is able to provide a lot of details, including marks that show an increase of flooding in certain areas and elevation information. The flood model presented in this paper is created using the found flood marks in drone imagery. The presented model is then compared to two commonly used flood models, and all three flood models are compared to locations of houses that collapsed from flooding throughout the refugee camp.

The model created using drone imagery did the best job predicting high risk locations with misclassification rates below 17%. The drone imagery model was then combined with a commonly used model to create a more comprehensive flood model, capitalizing on all available data.

Acknowledgements

This work could not have been done without the support of many people. I would first like to thank my advisor Dr. Kevin Kochersberger for his endless support and guidance, without him this work would have never been possible. I would also like to thank Dr. James Weeks and my committee members Dr. Venkat Sridhar and Dr. Michael Roan. Without the flood modeling support from Dr. Venkat Sridhar this work would not be where it is today.

Thank you to the African Drone and Data Academy Level 2 Cohort 1 class for collecting all of the drone imagery and Dzaleka Refugee Camp for allowing us to fly at the camp. This work would not have been possible without the surveying team including Ndapile Mkuwu, Regeza Kamungu, Espoir Bahirwe, and William Mufungizi. Thank you to UNICEF and Development Monitors for funding this work. Finally, thank you to my family and friends for your endless support and encouragement.

Table of Contents

1 Introduction

As climate change continues to occur, floods are having devastating effects on more and more communities, with a higher risk assigned to poorer communities that are ill-equipped for disaster response [1]. Flood modeling is an essential tool in enabling communities to reduce their vulnerability to flooding. Sadly, accurate flood modeling is still not accessible to everyone. The more commonly used flood models, hydrological-hydraulic based, use known mathematics that describe the hydrologic processes to create simulations, for example the water balance equation (i.e. used by SWAT), and mass and momentum conservation equations (i.e. used by HEC-RAS). Although these simulations have the potential to provide a lot of information about flooding in a study area, they require years of measured streamflow data and hydrology expertise to set model parameters and validate the model.

Some flood models are based on geological-geomorphological information, for example, finding out flood depth by studying the location of tree damage [2]. Although geological-geomorphological flood models don't have the same historical data requirements, they are currently not accessible due to the expertise they require (e.g. a dendrologist), not to mention the many working hours and special equipment needed. However, some geological-geomorphological information can be extracted from drone imagery and therefore does not have the same setbacks.

Drones and drone imaging technology is a fast-growing sector of data-driven analysis that accelerates collection and investigation of data, shrinking the digital divide that affects the most vulnerable populations disproportionately. The research presented in this thesis focuses on the use of drones to improve flood modeling accuracy, particularly for applications in the developing world. Drones are low-cost tools to accurately collect data, and combined with open-source or low-cost software it is possible to conduct flood modeling work for a fraction of the cost than what is found with larger-scale solutions.

Drones can very easily collect high-resolution images which can then be processed to create a digital terrain model (DTM) and orthomosaic, both of which are useful inputs for hydrological-hydraulic models and the geological-geomorphological flood model presented here. A high-resolution orthomosaic has significant geological-geomorphological information, some of which can provide evidence of flooding. For example, drone imagery can capture the change in water height of a stream through the change in bank color shown in an orthomosaic [3].

By using drone imagery collected at Dzaleka Refugee Camp in Dowa, Malawi, this paper presents a geological-geomorphological flood model based on erosion marks in the imagery. Some erosion marks provide information about historical flood events, if an erosion mark is water caused, then the mark is showing a location where water has run along the surface many times over a long period, and therefore provides a lot of information about flooding habits. We first compare the erosion marks found in the orthomosaic to flow direction to determine if the erosion marks are water caused. The flood model is then created by categorizing water caused erosion patterns (WCEP) and surrounding areas as high risk.

The proposed flood model is compared against two commonly used hydrological-hydraulic based models, the Soil & Water Assessment Tool (SWAT) and the Hydrologic Engineering Center River Analysis System (HEC-RAS).

The SWAT model is semi-distributed model that requires a digital terrain model (DTM), land use map, soil type information and climate data. The HEC-RAS model is fully distributed and requires a DTM, Manning's N map, precipitation data, and streamflow outlet velocity. Both of these models rely heavily on the precipitation data. The proposed WCEP model is an empirical model that only required information derived from the drone imagery.

By comparing the WCEP model to SWAT and HEC-RAS, we are able to determine how well our model predicts high risk flood areas. We are then also able to combine WCEP with the best hydrological-hydraulic flood model to create a hydrogeomorphological flood model, which in our case utilizes both the high-resolution drone imagery along with equations based on the hydrological process. The hydrogeomorphological approach has been found to be more consistent than just using the more typical hydrological-hydraulic method [4]. The hydrogeomorphological flood model is not only helpful for urban planning within a community, determining prime places for houses and agriculture, but also for determining flood risk regardless of the community's development stage. Table 1 provides a summary of the flood models used.

Table 1. Summary of flood models discussed in this paper.

Flood Model	Risk Model Abbreviation	Description
Soil & Water Assessment Tool (SWAT)	SR	Well-developed commonly used hydrological flood model. This paper uses surface runoff values output by SWAT to create the SR Flood Risk Model.
Hydrologic Engineering Center River Analysis System (HEC-RAS)	VE	Well-developed commonly used hydrological-hydraulic flood model. This paper uses water velocity values output by HEC-RAS to create the VE Flood Risk Model.
Water Caused Erosion Patterns (WCEP)	WCEP	Geological-geomorphological flood model, developed by the author to capitalize on high-resolution drone imagery. Based on erosion patterns found in the drone imagery that are water caused.
Hydrogeomorphological	--	Combination of the WCEP model and one of the other models (SR or VE) to take advantage of all available data. The hydrological-hydraulic model that performs better (SR or VE) is the one used.

2 Review of Literature

2.1 Types of Flood Modeling

Flood modeling enables people to understand and predict flood conditions which can reduce the negative impact floods have on communities. “In the last 20 years, more than 2.3 billion people were affected by floods,” making flood modeling even more crucial [5]. Over the years many flood models have been developed, and each one fills a different need. Three main categories can be used to define flood models: the structure, spatial resolution, and time scale [6].

2.2 Structure

A model's structure relates to how the output data is calculated, which can range from a black-box approach where the calculations rely on any relationship between known input and output data to a white-box approach where the calculations rely on the hydrological process. There are three main structures for flood modeling: empirical (black-box), conceptual (grey-box), and physically-based (white-box). Many flood models may take some attributes from multiple structures, but will still be categorized as the dominant structure used.

The simplest structure is an empirical model which uses a black-box approach to relate measured rainfall-runoff data [6]. The relation found can then be used to predict runoff values for any rainfall. Because of the black-box approach, empirical models are very reliant on the input observation data and the model does not account for hydrological processes [7]. The empirical structure is great for when both the input data and required output data are limited [8]. It is important to note that because empirical models don't account for the hydrological process, some measured data is required. Examples of models that use the empirical structure include regression equations, artificial neural networks, fuzzy logic, and HAZUS [8].

Conceptual models are in-between empirical and physically-based models in terms of complexity. Conceptual models take into account the hydrological process by using the water balance equations to convert the input (rainfall) to the output (runoff, evapotranspiration, and groundwater) [8]. Similar to empirical models, conceptual models don’t typically account for spatial variability and have a strong reliance on input data [9]. Examples of flood models that use the conceptual structure include the TOPMODEL, HBV, and HSPF [9].

The most computationally intense structure is physically-based which relates physics to the hydrological process by using the conservation of mass, momentum, and energy equations [8], [9]. Because model parameters are related to the physical characteristics of the study area, this structure is typically more realistic but this comes with the trade-off of greater data requirement [8]. Unlike the other two structures, a physically-based model requires data as a grid for the study area rather than a single averaged point. Examples of flood models that use a physically-based structure include SWAT, MIKE SHE, and HEC-RAS [9].

2.2.1 Spatial Resolution

The spatial resolution of a model defines the scale of the output data. Models can be lumped (Figure 1.a), semi-distributed (Figure 1.b), or fully-distributed (Figure 1.c).

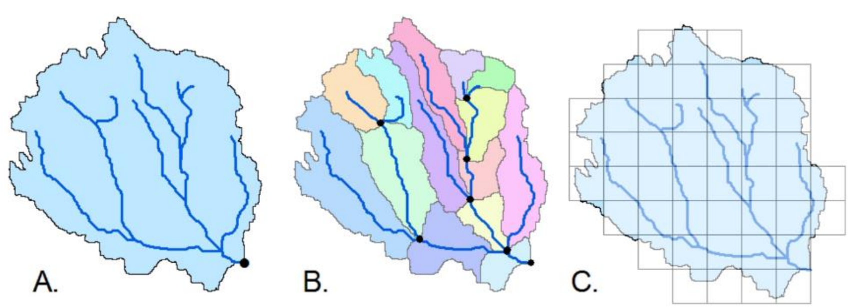

Figure 1. Three possible spatial resolutions for a flood model; (a) lumped, (b) semi-distributed, and (c) fully-distributed. Figure from [8].

The simplest resolution is lumped, where the study area is considered as one data point. Because of this simplification lumped models require low computation times and are good at producing study area averages, but the model does not account for spatial variability [8]. Lumped resolution is always used for empirical structures and sometimes used for conceptual structures. Figure 1.a is an example of lumped resolution where the model will only calculate output data for the single black dot.

Semi-distributed models have a resolution in-between lumped models and fully-distributed models. A model with semi-distributed resolution will break down the study area into sub-basins or group land with similar properties (i.e. land use, soil type, slope) together to provide output data for smaller units within the study area while still being computationally efficient. Semi-distributed resolution is sometimes used for conceptual or physically-based structures. Figure 1.b is an example of semi-distributed resolution, where the study area is split into sub-basins and the model will output a value (black dot) for each sub-basin.

The final type of spatial resolution used in flood modeling is fully-distributed. A fully-distributed model requires the most input data and is the most computationally intense, but provides the highest resolution of output data. A fully-distributed model breaks the study area into a grid and calculates hydrological variables for each cell taking into account the interactions with surrounding cells [8]. Fully-distributed models always use a physically distributed structure [8]. Figure 1.c provides an example of a fully-distributed model, where input values (i.e. land use, slope, soil, climate) would be required for each cell, and output values would be calculated for each cell.

2.2.2 Time Scale

The last category used to define flood models is the time scale. There are two types of time scales: event-based and continuous. Event-based models study a single precipitation-runoff event like a storm, while continuous models study a long period [6]. Event-based models provide more details about the short-term, and require sub-daily inputs (i.e. climate), while continuous models require years of data but on a larger scale (daily or weekly) [10].

2.3 Commonly Used Flood Models

There are many commonly used hydrology tools, Table 2 lists out seven different commonly used flood models. Please note that this is in no way an extensive list. To find out more about which hydrological models work best for certain situations please see [6], [9], [11], [12]. Below three models are discussed in more detail.

Table 2. Seven commonly used hydrology tools.

Model	Structure	Resolution	Time Scale	Open Source?	Source
Fuzzy Logic	Empirical	Lumped	Continuous or Even-Based	Yes	[13]
HAZUS	Empirical	--	Event	Yes	[14]
HEC-RAS	Physically Based	Fully-Distributed	Continuous	Yes	[15]
HSPF	Conceptual	Semi-Distributed	Continuous	Yes	[8]
MIKE-SHE	Physically Based	Fully-Distributed	Continuous and Event-Based	No	[16]
SWAT	Physically Based	Semi-Distributed	Continuous	Yes	[17]
TOPMODEL	Conceptual	Semi-Distributed	Continuous	---	[18]

2.3.1 Hydrological Simulating Program-FORTRAN

Hydrological Simulating Program-FORTRAN (HSPF) is an open-source, semi-distributed, continuous model that has been used in many studies [19]–[21], just to name a few. Ackerman et al. [19] studied the use of HSPF in two arid watersheds, Malibu and Ballona Creek, located in southern California. The Malibu watershed contains only about 4% of impervious surfaces while Ballona Creek is about 90% developed [19]. Ackerman et al. [19] input meteorological data, land use, terrain information, and streamflow measurements, along with nine years of rainfall and measured flow data. The first five years of the measured flow data were used for calibration and the following four years for validation. Ackerman et al. [19] found that HSPF can be used in arid climates especially when using a monthly or annual time scale, but the model does not accurately predict on a daily time scale during very dry conditions.

2.3.2 MIKE SHE

MIKE SHE is a commonly used hydrology model that is fully-distributed, physically-based, and can simulate both event-based or continuous time frames [16]. MIKE SHE has been used in many studies including [22]–[24]. Im et al. [22] quantitatively evaluated how the increase in urban development and decrease in natural vegetation impacts the hydrology of the Gyeongancheon watersheds in Korea. The MIKE SHE model requires rainfall data, evapotranspiration data, land use map, soil type, terrain data, and flow and water level information. Im et al. [22] use MIKE 11 to simulate flow and water level information, all other data was readily available for the study area. Im et al. [22] had four years of observed streamflow data at the outlet of the watershed, the first 2 years were used for calibration and the second 2 were used for validation. MIKE SHE was able to accurately simulate total runoff values but MIKE SHE underestimated peak flow during some rain events. The authors concluded their MIKE SHE model accurately depicted the watershed and therefore found that runoff and overland flow increased due to the reduction in natural vegetation and increase in urban development. To learn more about MIKE SHE please see the MIKE SHE User Manual [16].

2.3.3 Soil & Water Assessment Tool

Created in the early '90s, the Soil & Water Assessment Tool (SWAT) is an open-source, physically based, semi-distributed, continuous watershed model used in many published journal articles, [25]–[27] just to name a few. In [25], the authors explore how changes in land use affect hydrology in the River Njoro watershed in Kenya. SWAT requires climate data, a land use map, terrain data, and the soil types as inputs. Baker et al. [25] created three land use maps over a 17-year period and ran a SWAT simulation for each one and found that land-use changes occurring in their study area (i.e. deforestation, increase in cropland) increased surface runoff and decreased groundwater recharge.

2.4 Flood Model Data Collection via Drone

Drones are unmanned vehicles that fly, and with a sensor or product (i.e. camera, medicine, fertilizer, etc.) aboard the use cases for drones becomes limitless. There are two main types of drones: fixed-wing (Figure 2.a), and vertical takeoff and landing (VTOL) (Figure 2.b). Fixed-wing drones require more space to launch and recover, and also cannot hover in space, but they are more efficient allowing for longer flights with the ability to cover further distances. VTOL drones take off and land vertically so they require very little space for launch and recovery and they also can hover in space, but they are relatively inefficient and therefore cannot stay in the air as long. Typical drone endurance ranges from 10 minutes to 2 hours. This range accounts for drones of all different types and sizes along with having different payloads aboard. Table 3 lists out six different drones and their specifications.

(a) (b)

Figure 2. Example of the two main types of drones: (a) fixed-wing [28], and (b) VTOL [29].

Table 3. Comparison of six different drones.

Name	Drone Type	Weight (kg)	Max Flight Time (minutes)	Source
eBee X	Fixed-Wing	1.6	90	[30]
EcoSoar	Fixed-Wing	1.5	30	[31]
Mavic Air 2	VTOL- Quadcopter	.57	34	[32]
s500	VTOL- Quadcopter	1.25	20	[33]
Volantex 757-7 Ranger	Fixed-Wing	1	30	[28]
Wingcopter 178	VTOL- Can also fly as a fixed-wing	12	120	[34]

2.4.1 Drone Derived Products Used in Flood Modeling

Drones are becoming more popular to aid in flood modeling; one common use of drones for flood modeling is to create high-resolution digital terrain models (DTM). DTMs are required for many flood models, and are readily available for anywhere in the world through satellite imagery. But the resolution of a satellite-derived DTM is 30m, compared to a drone-derived DTM which can easily be less than 10cm. Backes et al. [5] used a DJI Phantom4 Professional drone to map an area in Dudelange, Luxembourg, the drone images were stitched together to make a 2cm resolution DTM. A flood model created using the drone imagery DTM was compared to a flood model created using a 1m resolution LiDAR DTM. Backes et al. [5] found that the microtopography picked up in the drone imagery DTM but not in the LiDAR DTM had a large positive effect on the accuracy of the flood model output. Rinaldi et al. [35] also found DTMs created from drone imagery to be very helpful for flood modeling.

Another common way for drones to aid in flood modeling is by creating real-time flood inundation maps. Loftis et al. [3] worked to enhance the flood preparedness of the Hampton Roads region in Virginia by using drone surveyed flood extents. An orthomosaic was created using captured drone imagery, and then edge detection was used on the orthomosaic to find the flooding extent at the time of flight. The edge detection would look for a change in color from dark (wet area) to light (dry area) pixels. Loftis et al. [3] found the flooding extent created from drone imagery to be comparable with ground-truthed and measured data. Baldazo et al. [36] has also found real-time flood inundation maps to be a great asset for flood modeling.

2.4.1.1 Drone Regulations and Flight Considerations

When planning a drone flight, it is crucial to understand the flight regulations for the area. Because drones are such a new technology, drone regulations don't exist in every country and in countries they do exist in, the regulations vary drastically. For example, in the United States to fly a drone under 55lb, a person only needs to pass a multiple-choice exam, but in Malawi you must pass a multiple-choice exam along with a practical flight test.

Areas of most interest for flood modeling are many times densely populated, causing it to be very difficult to avoid flying over people. This makes the flight even more hazardous and requires more pre-flight planning. Two important factors that should be considered when planning to fly over people, assuming the regulations allow it, are the size of the flight crew and the weight of the drone. When dealing with the public, it is important to have a large flight crew, this way the crew can support crowd control to ensure the flight is completed safely and reduce pilot distractions. This will only do so much though, assuming the drone malfunctions and falls out of the sky onto a person, the weight of the drone will reduce the injury and likelihood of death and therefore reduce the hazard.

3 Methodology

This section discusses the process used to create the Hydrogeomorphological Flood Model and Building Risk Map. An overview of the process is laid out in Figure 3, where purple represents collected input data, grey is intermediate processes (including the flood models (in blue)), green is collected evaluation data, and yellow are results.

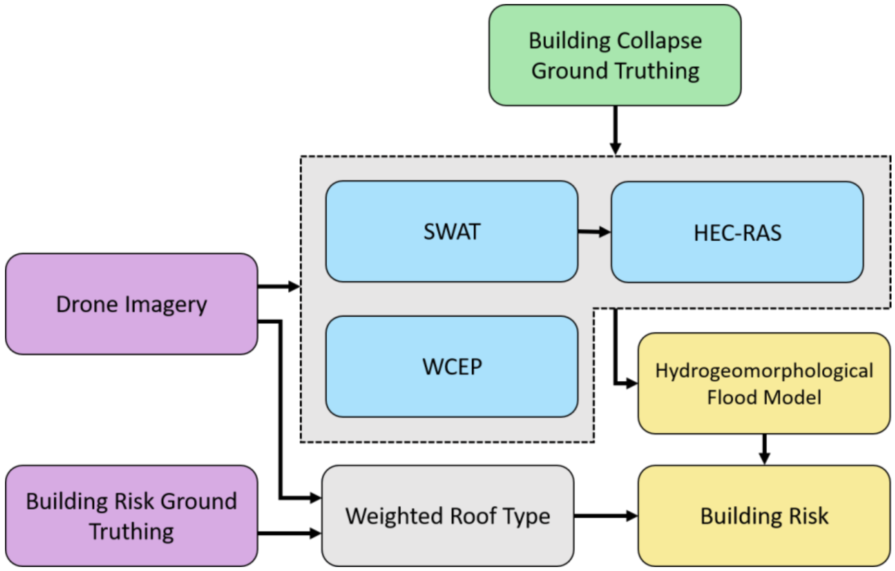

Figure 3. An overview of the process used to complete this work. Purple boxes are data sources, grey boxes are intermediate steps including flood models (blue), the green box is validation data and the yellow boxes are results.

Three different flood models have been created and compared, using free internationally available data along with drone imagery. Two of the flood models are commonly used, open-source, hydrological-hydraulic based models. The third model, Water Caused Erosion Patterns (WCEP), is a proposed methodology created by the author to capitalize on high-resolution drone imagery and overcompensate for the lack of other data. All three flood models are compared using the building collapse ground truthing data, which has locations of collapsed buildings from water-related events and therefore shows high-risk flood areas. The best hydrological-hydraulic flood model (SWAT or HEC-RAS) was combined with the WCEP model to create the Hydrogeomorphological Flood Model. The Hydrogeomorphological Flood Model supports the community with urban planning by showing the level of flood risk throughout Dzaleka Refugee Camp. Although the Hydrogeomorphological Flood Model is incredibly useful, it does not consider current building conditions.

To include the condition of current buildings in the flood model, a correlation needed to be drawn between structural integrity of a building and the building's roof type. This is because roof type can be classified in the drone imagery. Ground-truthing was completed to evaluate building risk, and to find correlations between building risk and roof type. The found correlations were used to create the Weighted Roof Type map which provided each building with a risk of collapse. Finally, the Weighted Roof Type map and Hydrogeomorphological Flood Model were combined to create the Building Risk Map, which evaluates the risk of collapse from water-related events of current structures.

3.1 Data Collection

This research focuses on data-scarce communities, so our method is based on low-cost drone imagery to create high resolution datasets. Along with drone imagery we also rely on easily collected ground-truthing, rather than historical measurements.

3.1.1 Ground Truthing

Drone imagery provides a lot of useful information, but is not enough to draw conclusions alone. Ground-truthing was paired with drone imagery to create our flood models. For this study, we have used two different ground-truthed data sets. The first was locations of houses that have collapsed from water-related events, which was a replacement for validation data. Validation data is used to evaluate how well a flood model represents the study area, this was exactly the use of the collapsed house data set. Collapsed house data points are high flood risk and so each flood model was evaluated on how well it reflected this. The app KoBoCollect [40] was used for surveyors to record the location of a collapsed house and the cause of the collapse. KoBoCollect automatically records horizontal accuracy, which is used when evaluating the models.

The second ground-truthed data source was building condition. The relationship between building condition and roof type was used to predict building conditions using drone imagery. The risk of building collapse was given one of three qualitative ratings: little to no risk of failure, risk of failure, and large risk of failure. Although these are qualitative ratings, all buildings were evaluated by one person so the comparison between buildings should be consistent.

3.1.2 Drone Imagery

Drones are becoming more and more accessible as their prices drop, and a cheap camera can take very high-resolution images when compared to satellite imagery (the alternative data source). Drone imagery can then be processed in a photogrammetry tool, stitching all of the images together to create a digital terrain model (DTM) and orthomosaic. Selecting the correct camera and planning an optimized mission have a large effect on the quality of the photogrammetry output.

Two important camera factors to consider are the camera resolution and the type of shutter. Camera resolution has a large effect on how much detail an image will show, the higher the resolution, the more detailed the image. There are two main types of camera shutters: rolling and global. Global shutters are very expensive, so for this work we focus on the use of a rolling shutter. Rolling shutters reduce the quality of the image, but some photogrammetry software, including Pix4Dmapper (the software used in this study), have a rolling shutter correction [37].

Depending on the speed of the drone, the camera may move a significant distance between the start and finish of image capture, this is because a rolling shutter will capture each image one line of pixels at a time [38]. To correct this, Pix4Dmapper approximates the location of each row of pixels using linear interpolation between the camera location at the start of capture and the camera location at the end of capture for an image. Figure 4 shows how processing works without (Figure 4.a) and with (Figure 4.b) the rolling shutter correction [38].

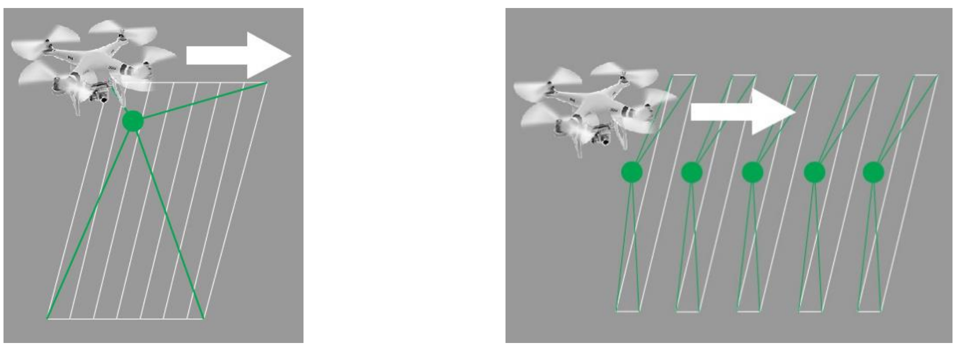

(a) (b)

Figure 4. (a) Pix4Dmapper method of processing without the rolling shutter correction (better to use for global shutters). (b) Pix4Dmapper rolling shutter correction, processing each row of pixels at a location specified by linear interpolation. Figure created by [38].

Vautherin et al. [39] compared three rolling shutter cameras to one global shutter camera each aboard a drone. Each rolling shutter data set was processed with and without the rolling shutter correction in Pix4Dmapper and compared to the global shutter data set. Six ground control points (GCPs) were used to georeferenced the reconstruction while another six GCPs were used for verification. Vautherin et al. [39] found that the rolling shutter correction greatly improved the results from rolling shutter data sets, especially as the drones increased in speed. When using the rolling shutter correction, the RMS error was reduced by an average of 66% when flying at 8 m/s for all three camera/drone setups.

Mission planning software (i.e. Pix4Dcapture, QGroundControl, and DroneDeploy) allows for the user to set multiple parameters, which can support optimizing flight time and image results. Some of the more important parameters are listed and described below.

- Flight Altitude: A higher flight altitude, allows for an area to be mapped faster, but the images will be lower resolution.
- Flight Speed: As a drone’s velocity increases, the speed of the mission increases, but if a drone flies too fast then the images will be blurry.
- Image Overlap: For accurately stitching images together, photogrammetry software requires image overlap. A higher imager overlap means more images are captured which can reduce the flight speed but improve photogrammetry output.

Once Pix4Dmapper created the DTM and orthomosaic, they were then be used as inputs for the flood models. A DTM provides elevation information, and many maps were derived from the DTM (i.e. slope and flow direction). The orthomosaic is a 2D RGB map and was used to create a land-use map, roof type map, and to extract geological-geomorphological information.

3.2 Flood Models

Three different flood models were used and evaluated in this study: the Soil & Water Assessment Tool (SWAT), the Hydrologic Engineering Center River System Analysis (HEC-RAS) and, Water Caused Erosion Patterns (WCEP). The three models were then compared and evaluated against the building collapse ground-truthing data. Finally, the best hydrological-hydraulic model (SWAT or HEC-RAS) was combined with the WCEP model to create the hydrogeomorphological flood model, which we believe will be more representative of flood risk. The hydrogeomorphological model capitalizes on all data available by using both the hydrological process and any hints of flooding found in the drone imagery. When working in a data-scarce area, capitalizing on all available data becomes even more important. Lastra et al. [4] found that hydrological-hydraulic methods tend to underestimate flood frequency, but when combined with geomorphological information the tendency for the model to underestimate reduces.

3.2.1 Soil & Water Assessment Tool (SWAT)

3.2.1.1 SWAT Overview

As discussed in Section 2.3, there are many flood modeling tools available, the Soil & Water Assessment Tool (SWAT) was one of the models selected for this study. In [41]–[44], the authors compared SWAT to other commonly used hydrology models and found SWAT to be the best open-source continuous model for a data-scarce area (similar to the area this study focuses on).

SWAT is a river basin or watershed scale model that was created to predict the effect that land management practices have on water, sediment, and agricultural chemical yields of an ungauged basin over a long time [45], [46]. Although originally developed by the United States Department of Agriculture, SWAT has created accurate models for watersheds all over the world [47]. A SWAT model is based on the water balance equation (Equation 1) [45].

$$SW_t = SW_0 + \sum_{i=1}^{t}(R_{day} - Q_{surf} - E_a - w_{seep} - Q_{gw}) \qquad \text{Equation 1}$$

"Where SW_t is the final soil water content (mm H_2O), SW_0 is the initial soil water content on day i (mm H_2O), t is the time (days), R_{day} is the amount of precipitation on day i (mm H_2O), Q_{surf} is the amount of surface runoff on day i (mm H_2O), E_a is the amount of evapotranspiration on day i (mm H_2O), w_{seep} is the amount of water entering the vadose zone from the soil profile on day i (mm H_2O), and Q_{gw} is the amount of return flow on day i (mm H_2O)."[45]

When modeling in SWAT, researchers use Nash-Sutcliffe Efficiency (NSE) (Equation 2) and Percent Bias (PBIAS) (Equation 3) statistical methods to evaluate the accuracy of the SWAT model output compared to observed values. NSE determines how well simulated and observed data will fit a 1:1 line by comparing the error variance of the model to the variance of the measured data. NSE ranges from -∞ to 1, where 1 is a perfect model [48], [49]. A satisfactory simulation should have an NSE > 0.5 [50]. PBIAS evaluates if the model tends to over or underestimate. A better model will have a low magnitude of PBIAS values (the optimal value is 0), while positive values indicate the model underestimating and negative values indicate the model overestimating [51]. The PBIAS value wanted to consider a model satisfactory depends on the variable of interest (i.e. -25% < PBIAS < 25% for streamflow and -55% < PBIAS < 55% for sediment) [50].

$$NSE = 1 - \frac{\sum_{i=1}^{n}(O_i - P_i)^2}{\sum_{i=1}^{n}(O_i - \bar{O})^2} \qquad \text{Equation 2}$$

$$PBIAS = \left[\frac{\sum_{i=1}^{n}(O_i - P_i)}{\sum_{i=1}^{n} O_i} * 100\right] \qquad \text{Equation 3}$$

In data-scarce areas, it can be impossible to calibrate SWAT and use NSE and PBIAS to evaluate SWAT. In [47], [52], [53], the authors compared calibrated and uncalibrated SWAT models to measured streamflow data using NSE and PBIAS and found that in many situations SWAT can be run without calibration.

Uzeika et al. [47] used an un-calibrated SWAT model to simulate runoff of a 1.19km^2 watershed (smaller than most watershed modeled using SWAT) located in southern Brazil. By comparing simulated values with hydro-sedimentological data, [47] found that SWAT inadequately modeled surface runoff daily (NSE averaging below -0.2), but the monthly simulation was satisfactory (NSE averaging above 0.45).

Niraula et al. [52] explored the importance of calibrating SWAT in the Santa Cruz River Watershed for forecasting absolute and relative changes in streamflow by comparing the outputs of three SWAT models each with varying degrees of calibration. The three degrees of calibration were:

- uncalibrated: default values used

- outlet-calibrated: model calibrated based on only the watershed outlet stream gauge (most commonly used)
- spatially-calibrated: model calibrated based on 14 gauges throughout the study area, including the watershed output

Using NSE and PBIAS, the observed flow was compared to the simulated flow on a monthly time scale. Although the uncalibrated model performed the worst, calibration didn't affect the relative change in streamflow due to precipitation or temperature. Niraula et al. [52] found that if the relative change is the factor of importance, results from an uncalibrated model are sufficient. In our study we are interested in comparing surface runoff at different points in the study area, relative to the average surface runoff throughout the study area, so relative change is the factor of importance.

Srinivasan et al. [53] evaluated the importance of SWAT calibration for the Upper Mississippi River Basin by comparing the calibrated model to the uncalibrated model, they found that the uncalibrated SWAT model produces similar results to calibrated models completed by three previous studies. Srinivasan et al. [53] determined that SWAT was able to meaningfully predict hydrologic budget and crop yield without calibration. Being able to use SWAT without calibration is not only important for ungauged watersheds, many times measured data has a lot of uncertainty [53].

3.2.1.2 SWAT Input Data

SWAT requires four input data sets: DTM, land use map, soil type, and daily climate data. The DTM and land use map were both derived from the drone imagery as discussed in section 3.1.1. The soil and climate data were both taken from, publicly available data sources, that cover the entire world.

The Harmonized World Soil Database (HWSD) is the only readily available soil database that covers the entire world by combing regional and national updates of soil information [54]. The soil data is very low resolution, with many of the data points being “filled in” through interpolation. Although low-resolution soil data is assumed to not be ideal, Geza et al. [55] compared SWAT outputs for the same study area using low (6.25km^2) and high (0.02km^2) resolution soil maps. Geza et al. [55] found that for their study area when SWAT was not calibrated, the simulation predicted more accurate streamflow values when using the low-resolution soil map compared to the high-resolution soil map. Although this study is only for one location, it supports the idea that a high-resolution soil map is not as necessary for uncalibrated SWAT simulations.

The climate data used for this study was taken from the National Centers for Environment Prediction Climate Forecast System Reanalysis (CFSR), which provides daily measurements of precipitation, temperature, wind, relative humidity, and solar radiation from 1979 – 2013 [56] for the entire world with a horizontal resolution of 38km. Fuka et al. [56] compared the SWAT output when using CFSR data to the SWAT output when using data from the closest weather station for five different watersheds. Fuka et al. [56] found that the SWAT model using CFSR generally had equal to or more accurate streamflow predictions.

3.2.1.3 SWAT Analysis

The main variable of interest for our study was surface runoff. "Surface runoff, or overland flow, is flow that occurs along a sloping surface,"[45] this water neither infiltrates the soil nor evaporates. SWAT provides surface runoff in mm of water which is the height of water running along the surface. SWAT has two methods for estimating surface runoff: the SCS Curve Number and the Green & Ampt Infiltration. The Green & Ampt Infiltration method was not an option for this study because it requires sub-daily precipitation data, which was unavailable for the study area.

The SCS Curve Number method is an empirical model created after over 20 years of studies exploring rainfall-runoff relationships from small rural watersheds across the US and computed using Equation 4.a [45].

$$Q_{surf} = \frac{\left(R_{day} - 0.2S\right)^2}{\left(R_{day} + 0.8S\right)} \qquad \text{Equation 4.a}$$

$$S = 25.4\left(\frac{1000}{CN} - 10\right) \qquad \text{Equation 4.b}$$

Where Q_{surf} is the accumulated surface runoff (mm H_2O), R_{day} is the daily rainfall depth (mm H_2O), and CN is the daily curve number which is a function of soil properties and land use. To determine CN, each soil type is placed into one of four categories based on the soil's infiltration characteristics. The U.S. Department of Agriculture provides tables to determine CN [57].

Once surface runoff was estimated using the SCS Curve Number method, the 10% exceedance probability values were mapped. The map was then normalized from 0 – 1 to create a flood risk map, where 0 is low risk and 1 is high risk.

3.2.2 Hydrologic Engineering Center River Analysis System (HEC-RAS)

3.2.2.1 (HEC-RAS) Overview

SWAT is an incredibly powerful tool, but it does not provide 2D hydrodynamic information like surface runoff velocity, so the Hydrologic Engineering Center River Analysis System (HEC-RAS) was also used. HEC-RAS can model 2-D unsteady flow hydraulics using the Shallow Water (SW) equations, which are a simplified version of the Navier-Stokes equations. SW assumes incompressible flow, uniform density, and hydrostatic pressure. HEC-RAS uses the mass conservation and momentum conservation equations. To learn more about how these equations are used in HEC-RAS see Chapter 2 of the HEC-RAS Hydraulic Reference Manual [15].

Two of the more important parameters set by the user are the mesh cell size and computational time step [58]. The mesh cell size is selected based on the complexity of the terrain and water flow, while the computational time step is selected based on the mesh size and maximum velocity. Choosing too small of a mesh cell size and computational time step leads to inefficient simulations, with very high computation times, while making the parameters too large creates a high volumetric accounting error (want error to be < 1%). The computational time step needs to be able to represent the change in boundary conditions (e.g. precipitation and flow hydrograph). The computational time step (ΔT) should be less than or equal to the mesh cell size (Δx) divided by the approximated (or guessed) maximum velocity (V) (Equation 5) [58].

$$\Delta T \leq \frac{\Delta x}{V} \qquad \text{Equation 5}$$

HEC-RAS 2D unsteady flow modeling outputs information that is incredibly useful for flood management, early warning systems, and land use development systems and many researchers have used HEC-RAS for just this, e.g. [59]–[61]. Output information from HEC-RAS (e.g. flood hazard map) can support the relocation of people, relocation of high-value crops, and creation of an emergency response plan [62]. The information can also be incredibly helpful for governments, non-profits, or NGOs to receive funding for natural disaster support.

3.2.2.2 HEC-RAS Input Data

To run HEC-RAS, boundary conditions including streamflow and precipitation into or out of the study area must be provided. Streamflow measurements are many times not available in data-scarce regions and would take years to collect. For this reason, we first analyzed the study area in SWAT and used SWAT's predicted outlet flow values as input boundary conditions for HEC-RAS. Many authors (e.g. [62], [63], [64]) have coupled SWAT and HEC-RAS to use an integrated approach to complete a hydrological-hydraulic flood model. Our coupling method was similar to the method used by Rivera et al. [62], who assessed the river flow patterns in the Aguan River Basin in Honduras to predict flood hazard areas. SWAT was used to predict discharge flow values at the river outlet, which was then used as a boundary condition for HEC-RAS. We used the same input precipitation data as used for SWAT.

HEC-RAS also requires 2 maps: DTM and manning's roughness coefficient. The same DTM map used in the SWAT model was used in HEC-RAS. Manning's roughness coefficient represents surface frictions [65] and was derived from a land-use map [66]. Manning's values were determined by using the conversion table provided in [66].

3.2.2.3 HEC-RAS Analysis

The variable of interest from HEC-RAS is surface velocity. Due to the computation time required to run HEC-RAS, only one month was simulated and a 20m mesh cell size was used. The month chosen was the one with the greatest rainfall accumulation. To ensure that Equation 5 was true the timestep used was one second, to make the program more efficient, the timestep could be increased in the future. The flood model was created by normalizing the max velocity map from 0 – 1, where 0 is low risk and 1 is high risk.

3.2.3 Water Caused Erosion Patterns (WCEP) Model

The final model used was the Water Caused Erosion Patterns (WCEP) Model which is the method proposed by the author to make up for the lack of data in data-scarce areas by taking advantage of high-resolution drone imagery and the geological-geomorphological information it can provide.

3.2.3.1 Introduction to Geological-Geomorphological Flood Modeling

Drone imagery has the potential to improve a hydrological flood model by providing geomorphological information. Geological-geomorphological flood modeling uses features on the earth's surface to support the determination of flood-prone areas. For example, [2] studied the historical flood events in Caldera de Taburiente National Park by using dendro-geomorphological data. Garrote et al. [2] collected samples of damaged trees to determine the approximate height and date of a past flood event, which was then combined with a hydrological model to create a more reliable flood hazard map. Garrote et al. [2] also found that “permanent high-water flood level markers on buildings can be used as additional data sources.”

Lioi et al. [67] compared the hydrologic-hydraulic method (typical flood model method) and the geological-geomorphological method to study Lama Lamasinata in southern Italy. The hydrologic-hydraulic method was completed using Flo-2D, while the geological-geomorphological method used two types of geomorphological descriptors. The two types of geomorphological descriptors were synthetic descriptors and composite descriptors. Synthetic descriptors are values like distance from the nearest stream and local slope, while composite descriptors are values like the modified topographic index (emphasizes areas exposed to flood inundation [68]) and the downslope index (estimates hydraulic gradient [69]). The geomorphological descriptors needed to be calibrated to determine their accuracy so the descriptors were normalized and then compared to a binary flooded reference map. Lioi et al. [67] found that the geomorphological method provided an equivalent output to the hydrologic-hydraulic method and sees the geomorphological method as a great tool for creating flood risk maps. Not only is the geological-geomorphological method many times faster it has also been found to be especially useful in data-scarce areas [4], [67].

3.2.3.2 WCEP Analysis

High-resolution drone imagery shows many geomorphological descriptors. We have focused on erosion marks more commonly found in bare earth areas. The process used to create the WCEP model from drone imagery is shown in Figure 5. Erosion marks are first found, and then compared to the flow direction to determine if they are water caused. Finally, the WCEPs are given a weight depending on how far they are from the original erosion mark. All of this is discussed more thoroughly below.

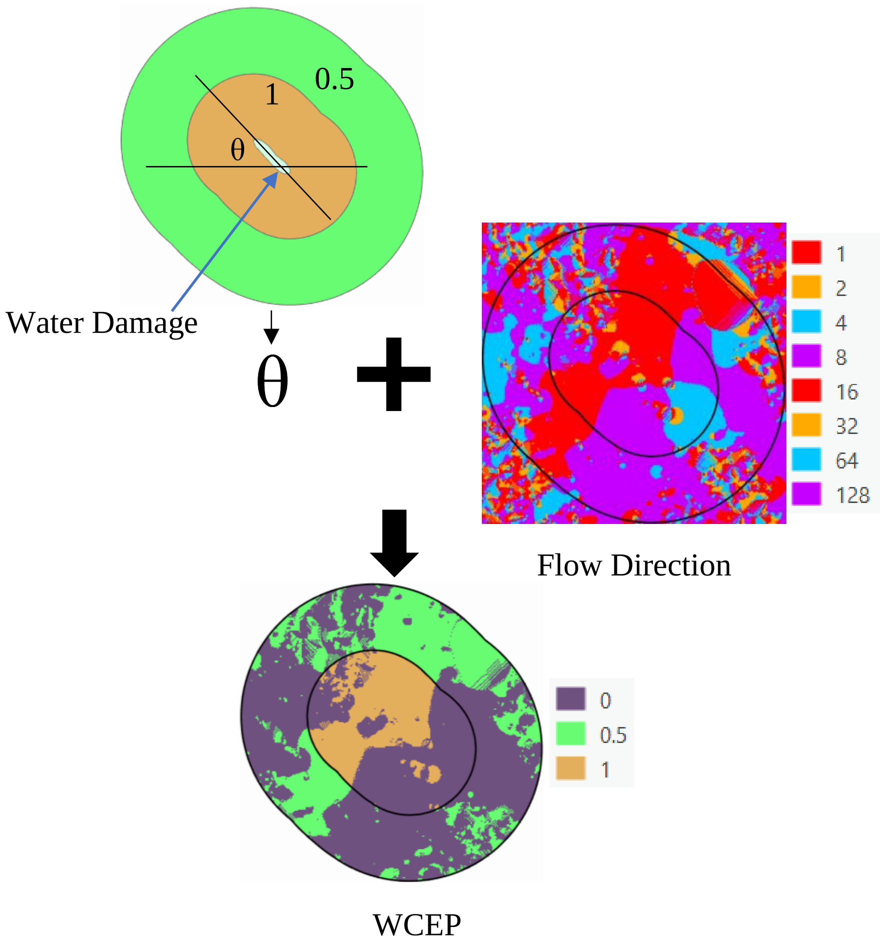

Figure 5. Process used to create the Water Cause Erosion Patterns (WCEP) model from the drone imagery.

An example of what erosion marks look like in drone imagery is shown in Figure 6.a, where the image on the right is zoomed in to emphasize the erosion marks which are the dark lines. Erosion marks have the potential to provide information about where there is a lot of water flow and therefore higher flood risk. To streamline the process, Picterra [70] a machine learning program, was trained to find these erosion patterns. Machine learning is commonly used to find features like oil spills, concrete cracks and water [71]–[73]. Figure 6.b is an example of a Picterra found erosion mark. The erosion patterns must be water caused to have any meaning for flood modeling, so erosion patterns were compared to flow direction (derived from the DTM). Each found erosion pattern was converted into a line (purple in Figure 7.a), and the flow direction of the erosion pattern (θ in Figure 7.a) was calculated using a compass reference. The flow direction of the erosion pattern was compared to a flow direction raster created using the D8 method on the DTM. The D8 method compares the elevation of a pixel to the elevation of all eight of its neighbors and then determines the direction water will flow. Each of the eight possible directions are given a number 1, 2, 4, 8, 16, 32, 64, and 128 (see Figure 7.b). If the erosion pattern was in the same direction as the flow then the line was considered a water-caused erosion pattern (WCEP). Table 4 provides the range of angles that correspond to each flow direction.

(a) (b)

Figure 6. Erosion patterns show up in drone imagery and then can be found using an AI program. (a) An example of a drone captured image at Dzaleka Refugee Camp along with an emphasis on the erosion patterns (dark lines) that Picterra (AI program) was trained to find. (b) An example of a Picterra found erosion pattern after training.

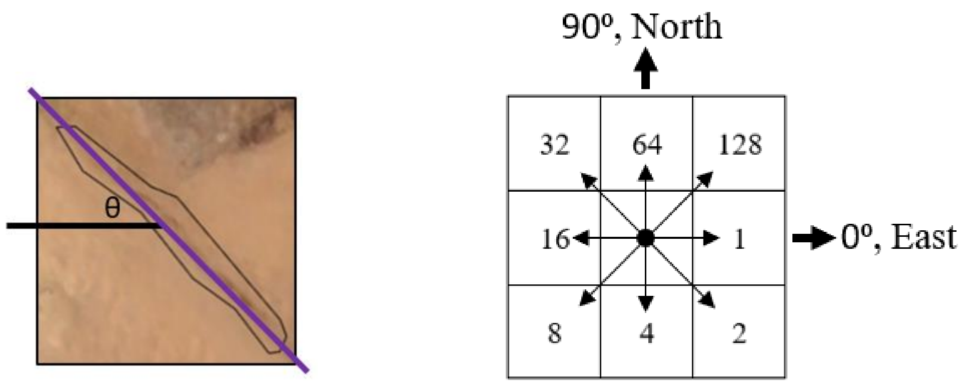

(a) (b)

Figure 7. (a) To compute the angle of each found erosion pattern, each polygon was converted into a line (purple) and then theta (θ) was calculated; (b) Based on the calculated theta, the flow direction is determined using the D8 flow direction method and the information in Table 4.

Table 4. Range of angles that correspond to each flow direction.

Flow Direction	Range of Degrees
1, 16	-45 → 45
2, 32	-90 → 0
4, 64	-90 → -45, 45 → 90
8, 128	0 → 90

Two buffers were also placed around each erosion pattern. This was to account for the fact that erosion patterns cannot occur where the earth is not bare (i.e. buildings). The first buffer was smaller and all WCEPs were given a weight of 1 within this buffer. The second buffer was double the diameter as the first and each WCEP was given a weight of 0.5. This is to account for the fact that as the distance from a WCEP increases, the risk of flooding decreases. The actual size of the buffer depends on the study area and how wide clusters of buildings (or other not bare earth) are. The final WCEP flood model contains values of 0, 0.5, and 1, where 0 is low risk and 1 is high risk.

3.2.4 Evaluation of Flood Models

Each of the three flood models were evaluated based on their correlation with houses that collapsed from different water-related events. A buffer was placed around each collapsed house data point to account for horizontal uncertainty. The average pixel value of a model within a buffer, z, was then used to calculate the misclassification rate which was the basis of model evaluation. The misclassification rate, $MR_{M,h}$, is calculated in Equation 6 where h is the reason for the collapse, and Y_M is the average value of model M. Y_M is used to calculate the misclassification rate to account for the different pixel value distributions of each model.

$$MR_{M,h} = \frac{\#\ of\ M_{z,h} < Y_M}{\#\ of\ M_{z,h}} * 100 \qquad \text{Equation 6}$$

3.3 Hydrogeomorphological Flood Model

The hydrological-hydraulic based model with the lowest misclassification rate was then combined with the WCEP model to make the Hydrogeomorphological Flood Model (HG), which should be a better representation of the study area than any single flood model. Equation 7 was used to combine the two best models, where c is a value between 0 and 1, $M1_z$ is the average Model 1 (either SWAT or HEC-RAS) value within the 5m buffer at collapsed house data point z, and $WCEP_z$ is the average WCEP model value within the 5m buffer at collapsed house data point z. The goal was to select a c-value that first minimized the train misclassification rate, then minimized the test misclassification rate, and finally maximized the train mean. A c-value was selected for each type of water-related house collapse by using cross-validation.

$$HG_z = c * M1_z + (1 - c) * WCEP_z \qquad \text{Equation 7}$$

Cross-validation splits data into two sets: training and testing to evaluate how well a system performs, this is done multiple times to optimize the model with little data. There are many methods of cross-validation, if a data-set had 10 data points or less the leave-one-out method was used, all other data sets used the Monte-Carlo method. The leave-one-out cross-validation method uses all but one data point in the train set [74]. This method runs the same number of times as there are data points, with each data point being the single test value. The Monte-Carlo 80/20 method randomly splits the data using 80% for training and the other 20% for testing, we did this 10 times. If the results were inconclusive, another five runs were completed. The Monte-Carlo method is non-exhaustive meaning that one data point could never be in the train or test set [74].

3.4 Roof Type and Building Risk

The hydrogeomorphological flood analysis provides an overview of flood risk throughout the study area, but it does not consider the current conditions of buildings. The Building Risk Map was created by multiplying the Weighted Roof Type map and the Hydrogeomorphological Flood Model. The Weighted Roof Type Map was created by first, using Picterra to classify roof types and then by combining roof type with the associated risk of building collapse (discussed in Sections 3.1.1). The Weighted Roof Type Map contains a weight for each roof found in the orthomosaic, the weight ranges from 0 – 1 and relates to the risk of collapse (0 = low risk, 1 = high risk). The Building Risk Map supports current residents in understanding the risk of their house collapsing from water related events, this way residents can plan ahead and reduce the likelihood of their house collapsing.

4 Results

4.1 Application of Methodology at Dzaleka Refugee Camp

4.1.1 Dzaleka Refugee Camp- Initial Data Collection and Flood Models

Located in Dowa, Malawi, Dzaleka Refugee Camp is home to 41,000 refugees from the Democratic Republic of Congo, Rwanda, Burundi, Ethiopia, and Somalia [75]. When they arrive, many refugees build a house out of concrete and home-made bricks created from dug-up clay. With little urban planning and poor building materials, refugees' homes encounter flood damage, and many homes collapse. Water events can cause buildings at Dzaleka to collapse in three different ways: foundation undermining (Figure 8.a), hydraulic pressure damage (Figure 8.b), and roof collapse due to water load (Figure 8.c). Foundation undermining occurs from water running along the dirt around the base of a structure, over time the dirt will wear away reducing the integrity of the structure's foundation. Hydraulic pressure damage occurs when water running along the surface applies pressure to the walls of a building causing the walls to collapse. Roof collapse due to water load occurs when the weight of rainfall is larger than the weight the roof can support. All three causes of building collapse can force Refugees to build their houses over and over again. In some cases, a collapsed house will even be abandoned by the owners, taking up precious space in an over-populated camp that was originally built for 10,000 people [75]. To combat the issues of flooding, drone imagery was used to create a flood model of Dzaleka Refugee Camp.

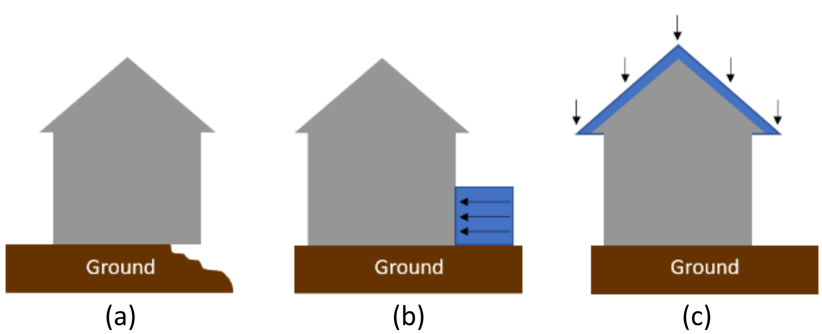

Figure 8. Buildings at Dzaleka Refugee Camp can collapse from water-related events in three different ways: (a) foundation undermining, (b) hydraulic pressure damage, and (c) roof collapse from water load.

4.1.1.1 Drone Imagery Collection and Processing

On March 19th, 2020, the African Drone & Data Academy completed a mapping mission over Dzaleka Refugee Camp (4.6 km^2) using a Parrot Disco drone with a Parrot Sequoia camera onboard (Figure 9). Appendix A provides documentation for approval of this flight. This study only used imagery from the RGB lens of the Sequoia. The RGB lens is a rolling shutter and has a resolution of 16MP, 4,608px x 3,456px. The mission was flown 120m above ground level with 70% image overlap. The mission took one day to complete and 2,603 RGB images were captured.

Figure 9. An African Drone and Data Academy student launching the Parrot Disco for the Dzaleka Refugee Camp mapping mission on March 19th, 2020.

After data collection, the images were stitched together in Pix4Dmapper using the rolling shutter correction and the Ag RGB processing template with minor modifications to the settings. Figure 11 shows an example of a drone image (left) along with the point cloud and image locations (right) created by Pix4Dmapper. See Appendix B for specific pix4Dmapper input settings. Pix4Dmapper built a digital terrain model (DTM) (Figure 11.a) and an RGB orthomosaic (Figure 11.b), both of which have a resolution of 3.5cm.

For much of the analysis, the DTM and RGB orthomosaic were resampled to 20cm resolution to reduce the processing power and time required.

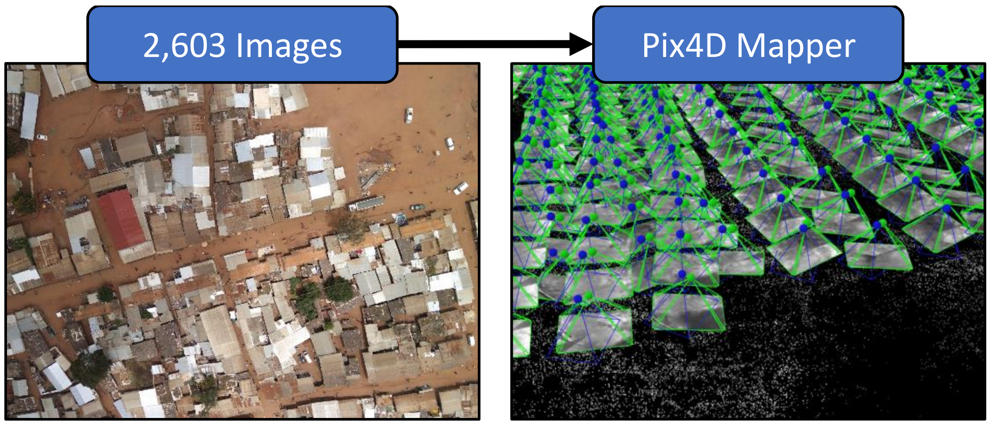

Figure 10. The process of creating a DTM and Orthomosaic in Pix4Dmapper. Starting with drone imagery (left) and then stitching the images together (right).

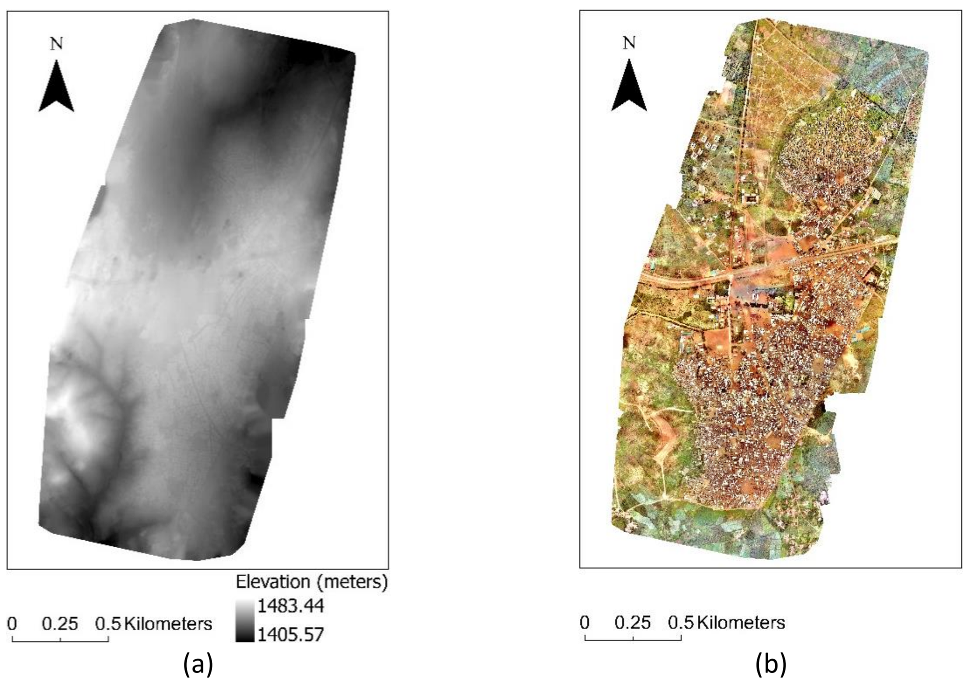

Figure 11. Initial maps of Dzaleka Refugee Camp created by Pix4D stitching flight images together; (a) Digital Terrain Model (DTM), and (b) Orthomosaic.

A land use map (Figure 12) was created using ArcGIS Classification Wizard tool on the 20cm resolution RGB orthomosaic. The notable settings used are listed below:

- Classification Method: Unsupervised
- Classification Type: Object Based
- Classification Schema: NLCD2011
- Maximum Number of Classes: 20

The created land-use map contained 20 different classes, the layer was then reclassified by combining similar classes. The final land use map is shown in Figure 12 and only contains the four classes seen at Dzaleka Refugee Camp: urban, bare, shrubland, and row crops. The 20cm resolution DTM, and 20cm resolution land use map were then used as inputs for the Soil and Water Assessment Tool (SWAT).

Figure 12. Land use map created by using ArcGIS Object Classification on the orthomosaic (Figure 11.b). The study area contains four different land classifications: urban (tan), bare (brown), shrubland (black), and row crops (green).

4.1.1.2 Soil & Water Assessment Tool (SWAT) Flood Model

As mentioned earlier, SWAT requires four data inputs: DTM, land use map, soil type and climate data. In HWSD Malawi's soil data is from the Soil and Terrain (SOTER) database which was initiated by the Food and Agricultural Organization of the UN in 1986 [76]. The resolution was 1km and many points were "filled in," meaning we don't know a lot about the soil type. SOTER classified the entire study area to have the same soil type with a dominant soil group of Lixisol. Lixisol soil is estimated to cover 14% of Africa and has a higher clay content in the subsoil than in the top soil, it is also prone to erosion and contains low levels of plant nutrients [77]. Climate data provided by CFSR was for a point 15.9km northwest from the center of camp located at -13.582 S, 33.750 E. The first four years were skipped for SWAT to "warm-up."

SWAT created 34 subbasins and 135 hydrological response units (HRU) for the study area, Figure 13.a shows the stream network (white lines), subbasins (black outlines), and HRUs (colors). An HRU (depicted in Figure 13.b, [78]) is a unique combination of subbasin, slope, land use, and soil type. Because the entire study area only has one soil type, for our case an HRU is a unique combination of subbasin, slope, and land use. SWAT is a semi-distributed model, so the highest resolution for output data is HRU-based.

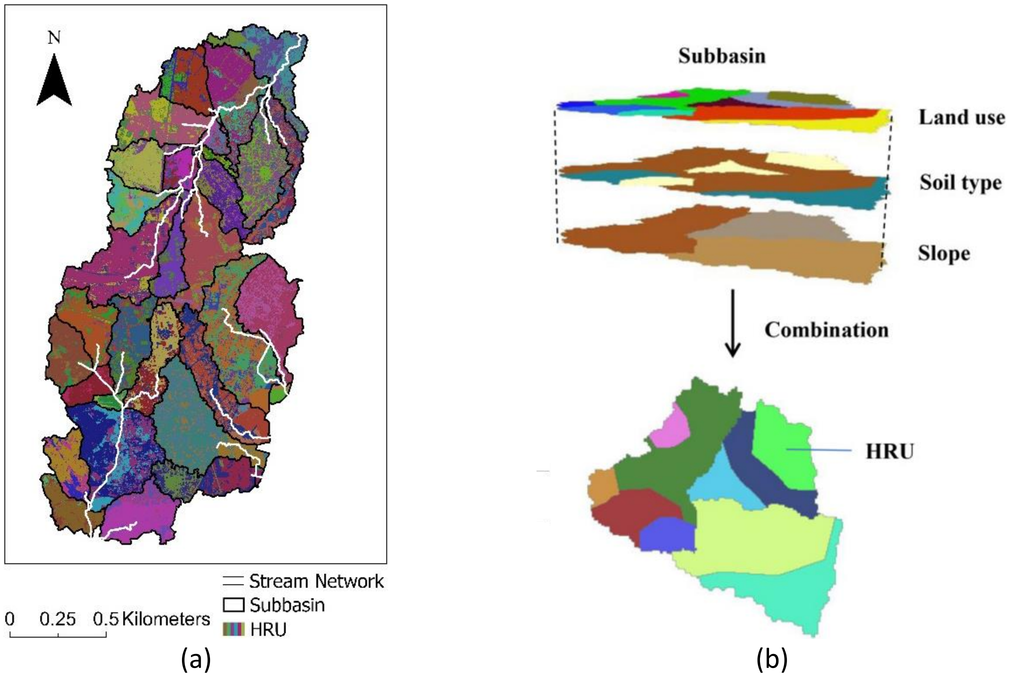

Figure 13. (a) Initial SWAT output for Dzaleka Refugee Camp. SWAT created 24 subbasins (black outline) based on the stream network (white lines), and 135 HRUs (colors). (b) Description of a hydrological response unit (HRU), created by [78].

From 1983 – 2013 the month with the greatest rain accumulation was January 2013, totaling 714mm of rain. The total generated surface runoff by HRU in January 2013 is shown in Figure 14.a. The surface runoff varies drastically throughout Dzaleka, ranging from 265.3mm to 479.5mm. Because of this large range, it is clear that some areas flood less than others and are therefore better equipped for homes. Instead of studying the worst event in recent history, the 10% surface runoff exceedance probability was analyzed, and again the study area experiences a large range of surface runoff. Figure 14.b is the 10% surface runoff exceedance probability for Dzaleka, the surface runoff ranges from 54.6mm to 181.2mm. Comparing surface runoff in January 2013 (Figure 14.a) to the 10% exceedance probability (Figure 14.b), it is clear that the amount of surface runoff in any particular HRU relative to the entire study area does not change. A flood risk map based on surface runoff (SR) was created by normalizing the 10% exceedance surface runoff probability map (Figure 14.b) from 0 to 1, where 1 is high flood risk and 0 is low flood risk. The SR model is shown in Figure 14.c.

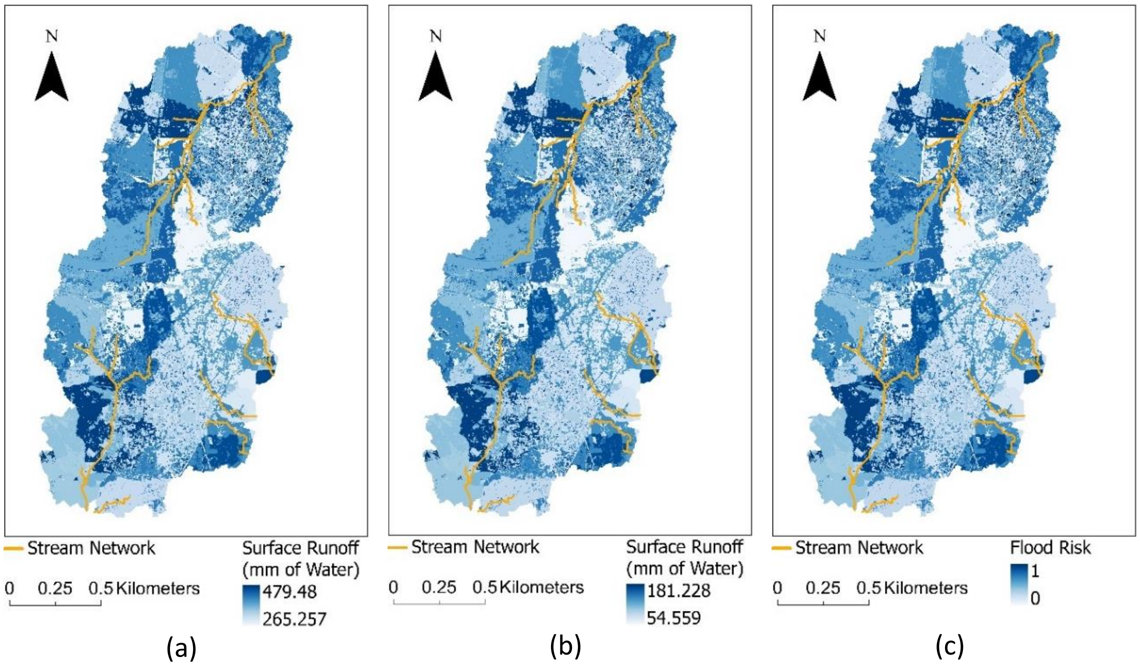

Figure 14. (a) Millimeters of water surface runoff accumulated in January 2013; (b) Millimeters of water surface runoff for a 10% exceedance event; (c) SR model which is the normalized version of Figure 14.b where 1 is high flood risk and 0 is low flood risk.

4.1.1.3 HEC-RAS Flood Model

HEC-RAS requires three data sets: DTM, manning's n and boundary conditions. The same DTM used in SWAT, was also used for HEC-RAS. Manning's n values were derived from the land use map used in SWAT, through the table provided by [66]. The manning's n values for the land use classifications found in our study area are summarized in Table 5.

Table 5. Manning's n values used for each of the four land uses found at Dzaleka Refugee Camp [66].

Land Use	Manning's N
Urban	0.08
Bare	0.025
Shrubland	0.1
Row Crop	0.035

There are many different boundary conditions that HEC-RAS can process. For this study three different types of boundary conditions were used: flow hydrograph, normal depth, and precipitation. Both flow hydrograph and normal depth boundary conditions are at the perimeter of the study area. It is necessary to place boundary conditions along the entire perimeter of the study area, because without them HEC-RAS will see the perimeter as a wall where water may not leave. The flow hydrograph represents the streamflow coming into or out of the study area. Being a data-scarce location, Dzaleka Refugee Camp does not have streamflow measurements, so the SWAT simulated streamflow measurements were used. Every cell along the perimeter that was not assigned to a flow hydrograph was considered a normal depth boundary condition. The normal depth boundary condition uses friction slope to evaluate flow into or out of the study area. We approximated all normal depth boundary condition cells to have a friction slope of 0.005. The final boundary condition used was precipitation, the precipitation data was taken from CFSR (same as SWAT) and provided daily rainfall measurements.

With all the input data sets prepared, we were able to run an unsteady flow analysis. Due to the computation time, our HEC-RAS simulation was only completed for one month, the month chosen was January 2013 because it had the greatest accumulation of rainfall.

The time step was one second and took about nine hours to run. After running, HEC-RAS approximated the volume accounting error to be 0.000779%.

Figure 15.a shows the maximum water velocity throughout the study area during January 2013, the velocity ranges from 0 to 4m/s. The velocity is of course greatest at the stream, which does not provide much information about flood risk on the surface throughout the camp. The greatest velocity outside of the stream network was 1.2m/s, so to create the HEC-RAS Velocity (VE) flood risk model Figure 15.a was normalized using 1.2 as the maximum value. All values above 1.2 in Figure 15.a were then reclassified to 1 for the VE model shown in Figure 15.b.

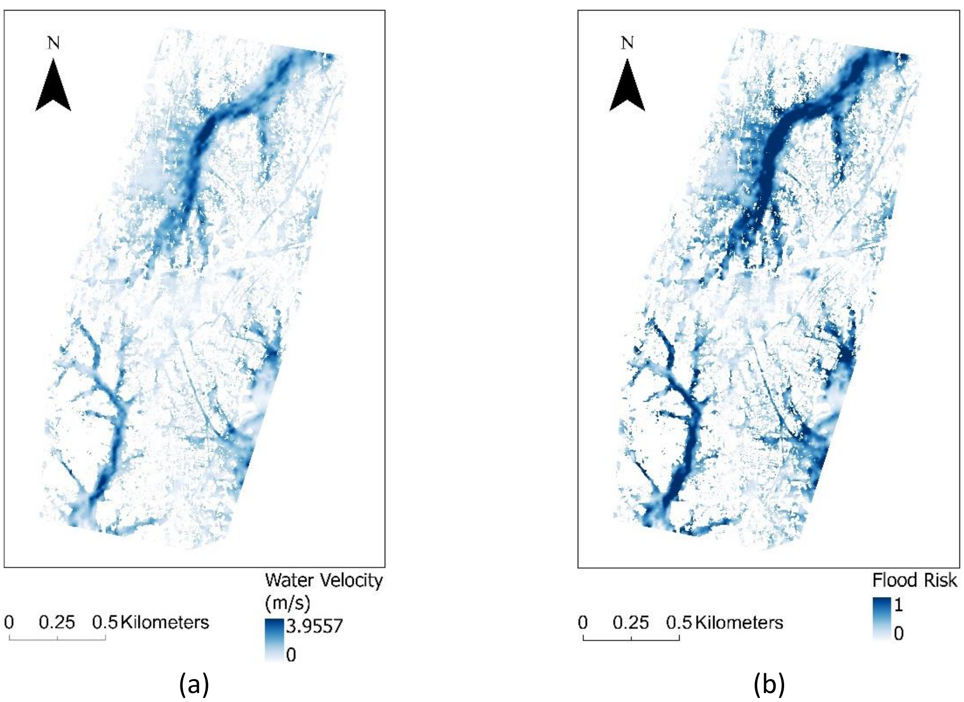

Figure 15. (a) Maximum surface velocity in January 2013, the surface velocity ranged from 0 – 4 meters per second. (b) VE flood risk model using HEC-RAS velocity.

4.1.1.4 Water Caused Erosion Patterns (WCEP) Flood Model

The 3.5cm resolution orthomosaic created by Pix4Dmapper was used in Picterra to find erosion marks (Figure 6). Houses are commonly found in clusters that can have a width up to about 40 meters, so buffers of 10 and 20 meters (a diameter of 20 and 40 meters respectively) were selected. Areas considered water caused in the 10 meter buffer were given a weight of 1, while areas considered water caused in the 20 meter buffer were given a weight of 0.5. This was done for the entire study area, which is shown in Figure 16.a. Figure 16.b shows a small portion of the study area to provide more detail about what the WCEP model looks like.

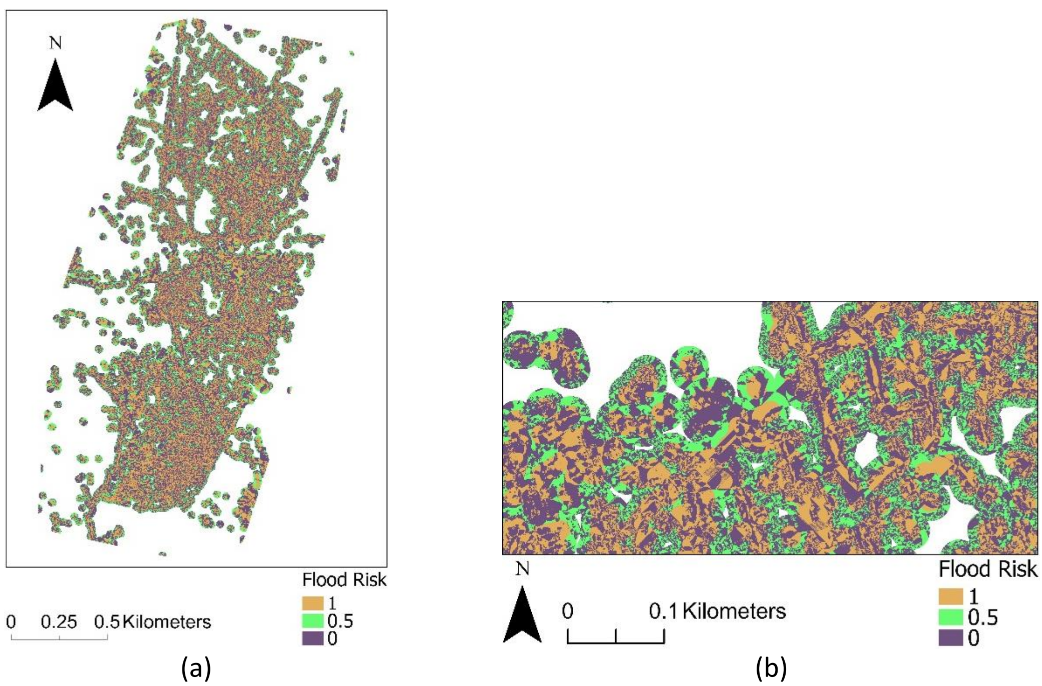

Figure 16. Water Caused Erosion Patterns (WCEP) model created by comparing Picterra found erosion marks with flow direction; (a) whole study area, (b) small section to provide more visual detail. Flood risk is 0 (purple), 0.5 (green) or 1 (orange).

4.1.2 Collapsed Houses Ground-Truthing for Evaluation of Flood Models

Ground-truthing of buildings that collapsed from water related events was completed by three surveyors. Prior to ground truthing the surveyors met with the author to discuss the procedures for ground truthing, the surveyors also received a write-up with details on the work which can be found in Appendix C.

Data was collected for 85% of the water-related collapsed houses in the study area, totaling 79 data points. Cause of collapse was determined through visual inspection or asking locals. Visual inspection for foundation undermining focused on finding eroded areas where the collapsed building stood, while visual inspection for hydraulic pressure damage focused on finding water marks on the walls. An example of each type of collapsed is shown in Figure 17.

Figure 17. Photo of each type of collapse found at Dzaleka Refugee Camp.

Table 6 summarizes how many data points were collected for each type of collapse. Figure 18 shows the distribution of the data collected, note that there is an area in the mid-west of Figure 18 that has no data points because half of it is a COVID-19 isolation area and the other half is public buildings. This data was collected for private houses only.

Table 6. Summary of collapsed house data points. The team collected a total of 79 data points.

Reason for Collapse	Number of Data Points
Foundation Undermining Figure 8.a	6
Hydraulic Pressure Damage Figure 8.b	28
Roof Collapse Figure 8.c	44
Other	1
Total	79

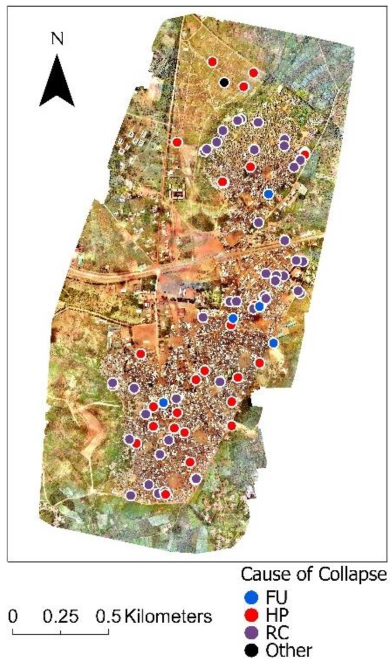

Figure 18. Distribution of 79 collected data points, where blue is foundation undermining (FU), red is hydraulic pressure damage (HP), purple is roof collapse (RC), and black is other.

The data point that was given “other” for reason of collapse has been neglected in all proceeding work because the reasoning for collapse was not water related, it was due to poor building materials. The data points categorized as “roof collapse” were also not used for evaluation of the flood models. This is because roof collapse is a function of precipitation only and precipitation is constant throughout the whole study area. The roof collapse data points may be useful for future research.

Most data points had a horizontal uncertainty of about 4 meters, and the maximum horizontal uncertainty was 4.9 meters so a 5-meter buffer was placed around each data point. Table 7 is a summary of the calculated values for each type of collapse (foundation undermining (FU), and hydraulic pressure damage (HP)) and flood model combination. It is clear from Table 7 that the WCEP model performs the best for representing locations at risk of collapse. The SR and VE models have fairly similar misclassification rates, but the SR model does better than the VE model for both types of collapse. A hydrogeomorphological flood model was created by combining the WCEP model with the best hydrological-hydraulic model (SR).

Table 7. Summary of how each model, m, performed for each type of collapse. FU is foundation undermining, and HP is hydraulic pressure damage.

m	SR	VE	WCEP
Y_m	0.389	0.188	0.251
$MR_{m,FU}$	50%	66.67%	16.67%
$MR_{m,HP}$	53.57%	57.14%	7.14%

4.1.2.1 Hydrogeomorphological Flood Model

Only six collapsed houses were caused by foundation undermining, so the leave-one-out cross validation method was run six times. Details of each run can be found in Appendix D. The optimal c value from every run was 0.339. Equation 8 is the optimal flood model to show locations at risk of foundation undermining and was used to create the Foundation Undermining Hydrogeomorphological Flood Model shown in Figure 19.a.

$$0.339 * SR_z + 0.661 * WCEP_z \qquad \text{Equation 8}$$

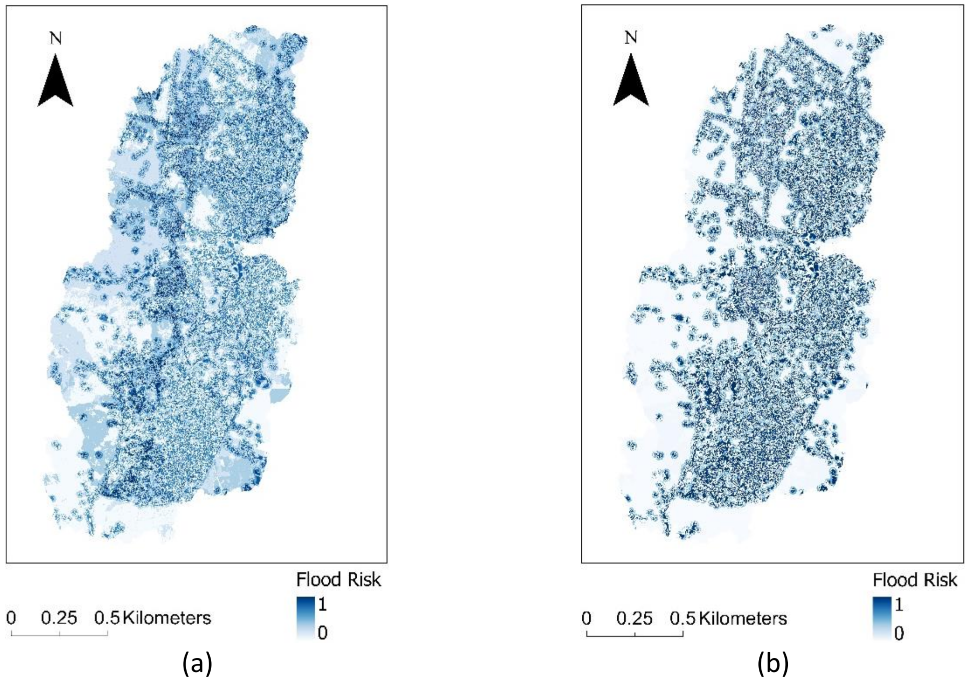

Figure 19. Flood risk for two different types of house collapse (1 = high risk, 0 = low risk) (a) Foundation Undermining Hydrogeomorphological Flood Model; (b) Hydraulic Pressure Damage Hydrogeomorphological Flood Model.

Hydraulic pressure damage had 28 data points, so the Monte Carlo cross validation method was used. Runs 1 – 10 were inconclusive, so 15 runs were completed in total. Table 8 lists the optimal c value calculated for each run. The optimal c value was 0.071 for the Hydraulic Pressure Damage Hydrogeomorphological Flood Model. Figure 19.b is the Hydraulic Pressure Damage Hydrogeomorphological Flood Model created using Equation 9. Appendix D has more data for each run.

Table 8. Optimal c value for each run. After the first 10 runs the optimal c value was inconclusive, so an addition five runs were completed.

Run	Optimal c value
1	0.071
2	0.074
3	0.071
4	0.071
5	0.39
6	0.071
7	0.074
8	0.071
9	0.02
10	0.074
11	0.071
12	0.071
13	0.071
14	0.071
15	0.071

$$0.071 * SR_z + 0.929 * WCEP_z \quad \text{Equation 9}$$

Because the c-value for both the foundation undermining dataset and the hydraulic pressure damage dataset is less than 0.5, it is clear that the WCEP model is more representative for both types of collapse compared to the SR model. Figure 20 is a box plot for the average pixel value at a collapsed house location for each of the four models: SWAT Surface Runoff (SR), HEC-RAS Velocity (VE), Water Cause Erosion Patterns (WCEP), and Hydrogeomorphological (HG). For both types of collapse (Figure 20.a and Figure 20.b) the WCEP and HG models have a much smaller distribution compared to the SR and VE models.

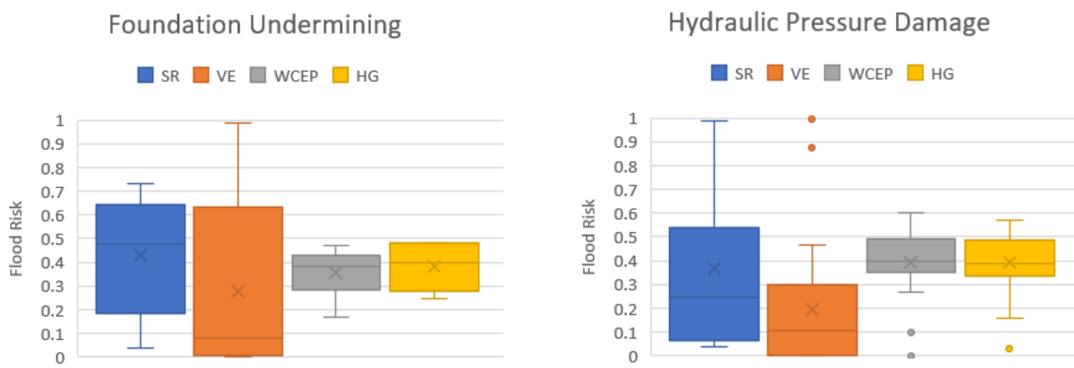

(a) (b)

Figure 20. Box plot of each model (SWAT Surface Runoff (SR), HEC-RAS Velocity (VE), Water Caused Erosion Patterns (WCEP), and Hydrogeomorphological (HG)) for two types of building collapses (foundation undermining and hydraulic pressure damage).

The HG model is incredibly useful for future urban planning. As new residents select plots to build, they can use the HG models to determine what type of collapse they are at most risk for, and focus their resources in recusing that risk. The HG model can also be used to determine great spots for agriculture (high flood locations), rather than houses, which could then also reduce flooding in surrounding areas.

The predictive capability of the HG model shown in this work is a great start to integrating drone imagery into flood modeling for a data-scarce location, but it should be improved in the future. More ground truthing needs to be done, with surveyors who have more training. If possible, the study area should also be monitored by locals and compared to the results in this paper, for further validation.

4.1.3 Relating Roof Type to Flood Risk

The drone imagery showed two types of roofs: tin and thatched. Figure 21 provides an example of each of these. Picterra was used to classify every building as tin or thatched in the orthomosaic, this is shown in Figure 22. Minimal ground truthing was done where the condition of 15 buildings were evaluated, Table 9 shares the findings. More ground-truthing needs to be completed, but from Table 9 it is clear that thatched roofs have a significantly higher risk of failure than tin roofs. We will approximate the risk of failure for thatched roofs to be about five times greater than tin roofs. To account for the difference in risk of collapse, tin roofs were given a weight of 0.2 and thatched roofs were given a weight of 1. This weight was then multiplied by each of the hydrogeomorphological flood models (Figure 19.a and Figure 19.b) to create two Building Risk Maps. Figure 23.a is the Foundation Undermining Building Risk Map, and Figure 23.b is the Hydraulic Pressure Damage Building Risk Map where 0 is low risk of collapse and 1 is high risk of collapse.

Figure 21. Examples of two types of roofing at Dzaleka Refugee Camp

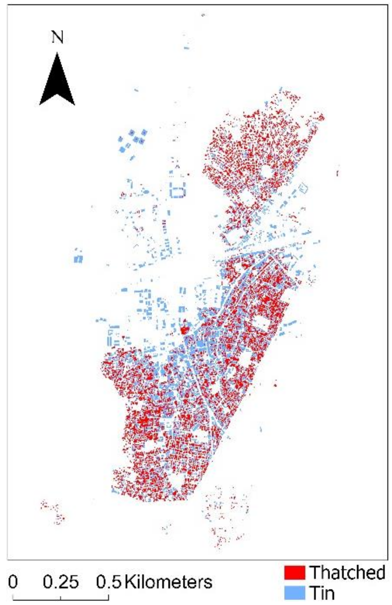

Figure 22. Picterra found buildings classified as tin (blue) or thatched (red).\

Table 9. Ground truthing of 15 buildings, comparing roof type to risk of building collapse.

Risk of Collapse	Thatched Roof	Tin Roof
Large Risk of Failure	6	0
Risk of Failure	2	1
Little to No Risk of Failure	2	4
Total	**10**	**5**

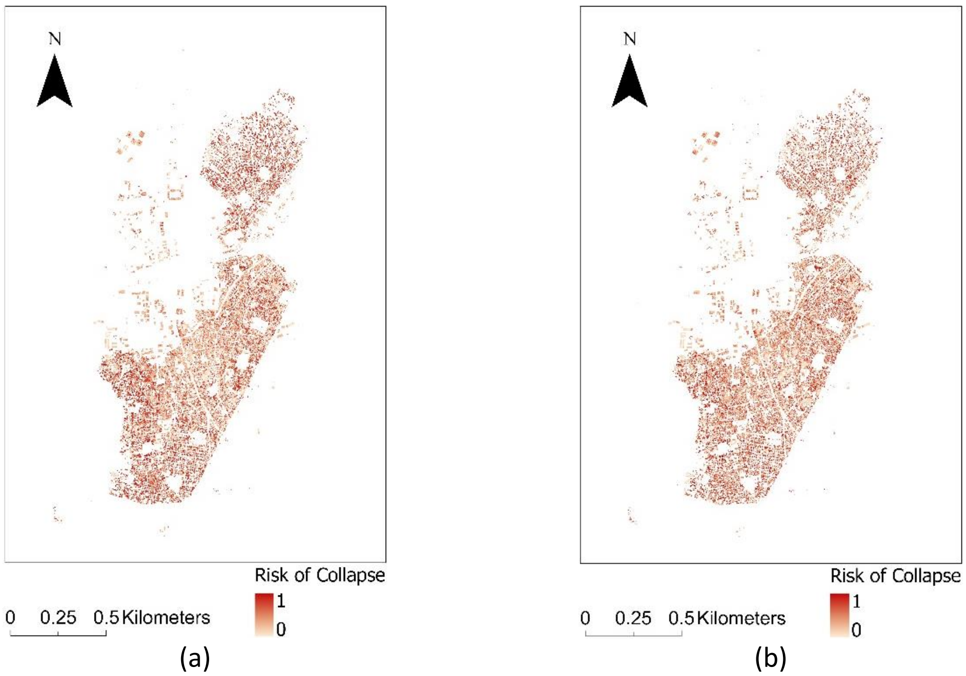

Figure 23. Building risk map for: (a) foundation undermining and (b) hydraulic pressure damage. (1 = high risk of collapse, 0 = low risk of collapse)

5 Discussion and Future Work

This work supports the idea that extracting flood features from drone imagery provides a cheap and meaningful alternative to hydrological-hydraulic flood models, especially for data-scarce communities. The Hydrogeomorphological Flood Models are able to support Dzaleka Refugee Camp with future urban planning. Not only do the Hydrogeomorphological Flood Models determine which locations are better equipped for houses, but they also provide information on precautions to take in high risk areas. For example, if you want to build in a location where the Foundation Undermining Hydrogeomorphological Flood Model shows high risk but the Hydraulic Pressure Hydrogeomorphological Flood Model shows low risk, the house should be built with a concrete floor, but does not necessarily need concrete reinforcing the walls. The hydrogeomorphological models are useful for future planning, but not very helpful for current residents. The Building Risk Map can be used to evaluate the risk of current buildings. Providing a warning to residents that their house is at a high risk of collapse, supports them in planning ahead.

In future work, more robust ground truthing should be collected for testing and validation. Due to COVID-19 and the fast-paced nature of this work, surveyors were given little training prior to ground truthing. For the building risk analysis ground truthing, the metrics should be made as quantitative as possible to reduce bias. This would also allow for more than one person to ground-truth, enabling more ground-truthing to be done. For the building collapse ground-truthing, surveyors should be shown multiple examples of each type of collapse, pointing out specific features to search for when determining the cause of collapse.

Not only does the ground-truthing need to become more robust, but more data is need. Six locations for houses that collapsed from foundation undermining is not enough. Similarly, only 15 buildings were analyzed to correlate building condition and roof type.

The soil type data and precipitation data should also be evaluated more. If higher resolution soil and precipitation data could be collected that would help evaluate their effect on the hydrological-hydraulic flood models. The data used was very low in resolution.

HEC-RAS should also be explored more, there are many settings and parameters that can be set to improve the model. Due to time, these parameters were not fully optimized. If

HEC-RAS is found to be a useful model, the set-up should be simplified so it is accessible to untrained users. This would allow for an open-source, user-friendly/accessible 2D flow simulation.

Finally, this study should be expanded to other communities. Comparing the results of a geomorphological model derived from drone imagery to a hydrological-hydraulic model for an area that is not data-scarce would help draw more conclusions on the accuracy of the geomorphological model.

References

[1] M. M. G. T. De Silva and A. Kawasaki, “Socioeconomic Vulnerability to Disaster Risk: A Case Study of Flood and Drought Impact in a Rural Sri Lankan Community,” *Ecological Economics*, vol. 152, pp. 131–140, Oct. 2018, doi: 10.1016/j.ecolecon.2018.05.010.

[2] J. Garrote, A. Díez-Herrero, M. Génova, J. M. Bodoque, M. A. Perucha, and P. L. Mayer, “Improving Flood Maps in Ungauged Fluvial Basins with Dendrogeomorphological Data. An Example from the Caldera de Taburiente National Park (Canary Islands, Spain),” *Geosciences*, vol. 8, no. 8, p. 300, Aug. 2018, doi: 10.3390/geosciences8080300.

[3] J. D. Loftis, H. Wang, D. Forrest, S. Rhee, and C. Nguyen, “Emerging flood model validation frameworks for street-level inundation modeling with StormSense,” in *Proceedings of the 2nd International Workshop on Science of Smart City Operations and Platforms Engineering*, New York, NY, USA, Apr. 2017, pp. 13–18, doi: 10.1145/3063386.3063764.

[4] J. Lastra, E. Fernández, A. Díez-Herrero, and J. Marquínez, “Flood hazard delineation combining geomorphological and hydrological methods: an example in the Northern Iberian Peninsula,” *Nat Hazards*, vol. 45, no. 2, pp. 277–293, May 2008, doi: 10.1007/s11069-007-9164-8.

[5] D. Backes, G. Schumann, F. N. Teferele, and J. Boehm, “Towards a High-resolution Drone-based 3d Mapping Dataset to Optimise Flood Hazard Modelling,” *The International Archives of the Photogrammetry, Remote Sensing and Spatial Information Sciences*, vol. XLII–2, no. W13, pp. 181–187, Jun. 2019.

[6] E. B. Daniel, J. V. Camp, E. J. LeBoeuf, J. R. Penrod, J. P. Dobbins, and M. D. Abkowitz, “Watershed Modeling and its Applications: A State-of-the-Art Review,” *The Open Hydrology Journal*, vol. 5, no. 1, pp. 26–50, Apr. 2011, doi: 10.2174/1874378101105010026.

[7] G. K. Devia, B. P. Ganasri, and G. S. Dwarakish, “A Review on Hydrological Models,” *Aquatic Procedia*, vol. 4, pp. 1001–1007, Jan. 2015, doi: 10.1016/j.aqpro.2015.02.126.

[8] J. Sitterson, C. Knightes, R. Parmar, K. Wolfe, M. Muche, and B. Avant, “Overview of Rainfall-Runoff Model Types,” United States Enviornmental Protection Agency, Office of Research and Development National Exposure Research Laboratory, 600R17482, May 2019. Accessed: Apr. 10, 2021. [Online]. Available: https://nepis.epa.gov/Exe/ZyNET.exe/P100WLPI.txt?ZyActionD=ZyDocument&Client=EPA&Index=2016%20Thru%202020&Docs=&Query=&Time=&EndTime=&SearchMethod=1&TocRestrict=n&Toc=&TocEntry=&QField=&QFieldYear=&QFieldMonth=&QFieldDay=&UseQField=&IntQFieldOp=0&ExtQFieldOp=0&XmlQuery=&File=D%3A%5CZYFILES%5CINDEX%20DATA%5C16THRU20%5CTXT%5C00000011%5CP100WLPI.txt&User=ANONYMOUS&Password=anonymous&SortMethod=h%7C-&MaximumDocuments=1&FuzzyDegree=0&ImageQuality=r75g8/r75g8/x150y150g16/i425&Display=hpfr&DefSeekPage=x&SearchBack=ZyActionL&Back=ZyActionS&BackDesc=Results%20page&MaximumPages=1&ZyEntry=2.

[9] R. K. Jaiswal, S. Ali, and B. Bharti, “Comparative evaluation of conceptual and physical rainfall–runoff models,” *Appl Water Sci*, vol. 10, no. 1, p. 48, Jan. 2020, doi: 10.1007/s13201-019-1122-6.

[10] D. Yu *et al.*, “Improvement of the SWAT model for event-based flood simulation on a sub-daily timescale,” *Hydrology and Earth System Sciences*, vol. 22, no. 9, pp. 5001–5019, Sep. 2018, doi: 10.5194/hess-22-5001-2018.

[11] G. Liangliang and L. Daoliang, “A review of hydrological/water-quality models,” *Front. Agr. Sci. Eng.*, vol. 1, no. 4, pp. 267–276, Mar. 2015, doi: 10.15302/J-FASE-2014041.

[12] F. Unduche, H. Tolossa, D. Senbeta, and E. Zhu, “Evaluation of four hydrological models for operational flood forecasting in a Canadian Prairie watershed,” *Hydrological Sciences Journal*, vol. 63, no. 8, pp. 1133–1149, Jun. 2018, doi: 10.1080/02626667.2018.1474219.

[13] S. Kambalimath and P. C. Deka, “A basic review of fuzzy logic applications in hydrology and water resources,” *Appl Water Sci*, vol. 10, no. 8, p. 191, Jul. 2020, doi: 10.1007/s13201-020-01276-2.

[14] F. Antolini, E. Tate, B. Dalzell, N. Young, K. Johnson, and P. L. Hawthorne, “Flood Risk Reduction from Agricultural Best Management Practices,” *JAWRA Journal of the American Water Resources Association*, vol. 56, no. 1, pp. 161–179, 2020, doi: https://doi.org/10.1111/1752-1688.12812.

[15] G. Brunner, “HEC-RAS River Analysis System Hydraulic Reference Manual,” US Army Corps of Engineers, Computer Program Documentation CPD-69, Dec. 2020. [Online]. Available: https://www.hec.usace.army.mil/software/hec-ras/documentation/HEC-RAS%205.0%20Reference%20Manual.pdf.

[16] “MIKE SHE User Manual Volume 1: User Guide.” DHI Water & Environment, Nov. 10, 2006.

[17] “SWAT | Soil & Water Assessment Tool,” *Soil & Water Assessment Tool*. https://swat.tamu.edu/ (accessed Feb. 12, 2021).

[18] K. Beven, “TOPMODEL: A critique,” *Hydrological Processes*, vol. 11, no. 9, pp. 1069–1085, 1997, doi: https://doi.org/10.1002/(SICI)1099-1085(199707)11:9<1069::AID-HYP545>3.0.CO;2-O.

[19] D. Ackerman, K. C. Schiff, and S. B. Weisberg, “Evaluating HSPF in an Arid, Urbanized Watershed,” *JAWRA Journal of the American Water Resources Association*, vol. 41, no. 2, pp. 477–486, 2005, doi: https://doi.org/10.1111/j.1752-1688.2005.tb03750.x.

[20] P. B. Duda, P. R. Hummel, A. Jr. S. Donigian, and J. Imhoff, “BASINS/HSPF: Model Use, Calibration, and Validation,” *Transactions of the ASABE*, vol. 55, no. 4, pp. 1523–1547, Jun. 2012.

[21] M. Albek, Ü. Bakır Öğütveren, and E. Albek, “Hydrological modeling of Seydi Suyu watershed (Turkey) with HSPF,” *Journal of Hydrology*, vol. 285, no. 1, pp. 260–271, Jan. 2004, doi: 10.1016/j.jhydrol.2003.09.002.

[22] S. Im, H. Kim, C. Kim, and C. Jang, “Assessing the impacts of land use changes on watershed hydrology using MIKE SHE,” *Environ Geol*, vol. 57, no. 1, p. 231, Apr. 2008, doi: 10.1007/s00254-008-1303-3.

[23] J. R. Thompson, H. R. Sørenson, H. Gavin, and A. Refsgaard, “Application of the coupled MIKE SHE/MIKE 11 modelling system to a lowland wet grassland in southeast England,” *Journal of Hydrology*, vol. 293, no. 1, pp. 151–179, Jun. 2004, doi: 10.1016/j.jhydrol.2004.01.017.

[24] R. Singh, K. Subramanian, and J. C. Refsgaard, “Hydrological modelling of a small watershed using MIKE SHE for irrigation planning,” *Agricultural Water Management*, vol. 41, no. 3, pp. 149–166, Aug. 1999, doi: 10.1016/S0378-3774(99)00022-0.

[25] T. Baker and S. Miller, “Using the Soil and Water Assessment Tool (SWAT) to assess land use impact on water resources in an East African watershed,” *Journal of Hydrology*, vol. 486, pp. 100–111, Apr. 2013, doi: 10.1016/j.jhydrol.2013.01.041.

[26] G. Ghaffari, S. Keesstra, J. Ghodousi, and H. Ahmadi, “SWAT-simulated hydrological impact of land-use change in the Zanjanrood basin, Northwest Iran,” *Hydrological Processes*, vol. 24, no. 7, pp. 892–903, 2010, doi: https://doi.org/10.1002/hyp.7530.

[27] T. Aawar and D. Khare, “Assessment of climate change impacts on streamflow through hydrological model using SWAT model: a case study of Afghanistan,” *Model. Earth Syst. Environ.*, vol. 6, no. 3, pp. 1427–1437, Sep. 2020, doi: 10.1007/s40808-020-00759-0.

[28] “Volantex 757-7 Ranger (PNF) 1600mm FPV Glider (63"),” *Hobbyking*. https://hobbyking.com/en_us/volantex-757-7-ranger-1600mm-fpv-glider-63-pnf.html?wrh_pdp=2 (accessed Apr. 13, 2021).

[29] “Pixhawk4 S500 KIT,” *Holybro*. http://www.holybro.com/product/pixhawk4-s500-kit/ (accessed Apr. 13, 2021).

[30] “eBee X Fixed-Wing Mapping and Surveying Drone,” *senseFly*, Sep. 04, 2018. https://www.sensefly.com/drone/ebee-x-fixed-wing-drone/ (accessed Apr. 13, 2021).

[31] Z. Standridge, “Design and Development of Low-cost Multi-function UAV Suitable for Production and Operation in Low Resource Environments,” Virginia Tech, 2018.

[32] “Mavic Air 2 - Specifications - DJI,” *DJI Official*. https://www.dji.com/mavic-air-2/specs (accessed Apr. 13, 2021).

[33] “ADDA User Manual for S500 V2 Quadcopter- Revision 3.” Oct. 22, 2019.

[34] “Technical Details- Wingcopter 178 Heavy Lift A (Delivery Variant) Version 01-2021.” Wingcopter, [Online]. Available: https://wingcopter.com/wp-content/uploads/2021/02/Technical-Details-Wingcopter-178-Heavy-Lift-A-Delivery-Variant-1-1.pdf.

[35] P. Rinaldi, I. Larrabide, and J. P. D’Amato, “Drone Based DSM Reconstruction for Flood Simulations in Small Areas: A Pilot Study,” in *New Knowledge in Information Systems and Technologies*, Cham, 2019, pp. 758–764, doi: 10.1007/978-3-030-16181-1_71.

[36] D. Baldazo, J. Parras, and S. Zazo, “Decentralized Multi-Agent Deep Reinforcement Learning in Swarms of Drones for Flood Monitoring,” in *2019 27th European Signal Processing Conference (EUSIPCO)*, Sep. 2019, pp. 1–5, doi: 10.23919/EUSIPCO.2019.8903067.

[37] “Pix4Dmapper,” *Pix4D*. https://www.pix4d.com/product/pix4dmapper-photogrammetry-software (accessed Apr. 17, 2021).

[38] “Improved accuracy for rolling shutter cameras,” *Pix4D*, Apr. 20, 2016. /blog/rolling-shutter-correction (accessed Mar. 16, 2021).

[39] J. Vautherin *et al.*, “Photogrammetric Accuracy and Modeling of Rolling Shutter Cameras,” *ISPRS Annals of Photogrammetry, Remote Sensing and Spatial Information Sciences*, vol. III–3, pp. 139–146, Jun. 2016, doi: 10.5194/isprsannals-III-3-139-2016.

[40] “Projects | KoboToolbox.” https://kobo.humanitarianresponse.info/#/forms (accessed Apr. 15, 2021).

[41] M. Van Liew, J. Arnold, and J. Garbrecht, “Hydrologic Simulation on Agricultural Watersheds: Choosing Between Two Models,” *American Society of Agricultural and Biological Engineers*, vol. 46, no. 6, pp. 1539–1551, Jul. 2003.

[42] D. Borah and M. Bera, “Watershed-Scale Hydrologic and Nonpoint-Source Pollution Models: Review of Mathematical Bases,” *American Society of Agricultural and Biological Engineers*, vol. 46, no. 6, pp. 1553–1566, Sep. 2003.

[43] A. Saleh and B. Du, “Evaluation of SWAT and HSPF within Basins Program for the Upper North Bosque River Watershed in Centeral Texas,” *American Society of Agricultural and Biological Engineers*, vol. 47, no. 4, pp. 1039–1049, Apr. 2004.

[44] D. Nguyen Khoi, “Comparison of the HEC-HMS and SWAT Hydrological Models in Simulating the Streamflow,” *Journal of Science and Technology*, vol. 53, no. 5A, pp. 189–195, Nov. 2015.

[45] S. L. Neitsch, J. Arnold, J. R. Kiniry, and J. R. Williams, “Soil and Water Assessemt Tool Theoretical Documentation Version 2009,” Texas Water Resources Institute Technical Report, Texas A&M University System, College Station, Texas, 406, Sep. 2011.

[46] P. Gassman, M. Reyes, C. Green, and J. Arnold, “The Soil and Water Assessment Tool: Historical Development, Applications, and Future Research Directions,” *American Society of Agricultural and Biological Engineers*, vol. 50, no. 4, pp. 1211–1250, May 2007.

[47] T. Uzeika, G. H. Merten, J. P. G. Minella, and M. Moro, “Use of the swat model for hydro-sedimentologic simulation in a small rural watershed,” *Revista Brasileira de Ciência do Solo*, vol. 36, no. 2, pp. 557–565, Apr. 2012, doi: 10.1590/S0100-06832012000200025.

[48] J. Nash and J. Sutcliffe, “River flow forecasting through conceptual models part I — A discussion of principles,” *Journal of Hydrology*, vol. 10, no. 3, pp. 282–290, Apr. 1970, doi: 10.1016/0022-1694(70)90255-6.

[49] G. Tegegne, D. K. Park, and Y.-O. Kim, “Comparison of hydrological models for the assessment of water resources in a data-scarce region, the Upper Blue Nile River Basin,”

Journal of Hydrology: Regional Studies, vol. 14, pp. 49–66, Dec. 2017, doi: 10.1016/j.ejrh.2017.10.002.

[50] D. Moriasi, J. Arnold, M. Van Liew, R. Bingner, D. Harmel, and T. Veith, “Model Evaluation Guidelines for Systematic Quantification of Accuracy in Watershed Simulations,” *American Society of Agricultural and Biological Engineers*, vol. 50, no. 3, pp. 885–900, Mar. 2007.

[51] H. V. Gupta, S. Sorooshian, and P. O. Yapo, “Status of Automatic Calibration for Hydrologic Models: Comparison with Multilevel Expert Calibration,” *Journal of Hydrologic Engineering*, vol. 4, no. 2, pp. 135–143, Apr. 1999, doi: 10.1061/(ASCE)1084-0699(1999)4:2(135).

[52] R. Niraula, T. Meixner, and Norman, “Determining the importance of model calibration for forecasting absolute/relative changes in streamflow from LULC and climate changes,” *Journal of Hydrology*, vol. 522, pp. 439–451, Mar. 2015, doi: 10.1016/j.jhydrol.2015.01.007.

[53] R. Srinivasan, X. Zhang, and J. Arnold, “SWAT Ungauged: Hydrological Budget and Crop Yield Predictions in the Upper Mississippi River Basin,” *American Society of Agricultural and Biological Engineers*, vol. 53, no. 5, pp. 133–1546, May 2010.

[54] “Harmonized world soil database v1.2 FAO SOILS PORTAL,” *Food and Agriculture Organization of the United Nations*. http://www.fao.org/soils-portal/data-hub/soil-maps-and-databases/harmonized-world-soil-database-v12/en/ (accessed Feb. 14, 2021).

[55] M. Geza and J. E. McCray, “Effects of soil data resolution on SWAT model stream flow and water quality predictions,” *Journal of Environmental Management*, vol. 88, no. 3, pp. 393–406, Aug. 2008, doi: 10.1016/j.jenvman.2007.03.016.

[56] D. R. Fuka, M. T. Walter, C. MacAlister, A. T. Degaetano, T. S. Steenhuis, and Z. M. Easton, “Using the Climate Forecast System Reanalysis as weather input data for watershed models: USING CFSR AS WEATHER INPUT DATA FOR WATERSHED MODELS,” *Hydrol. Process.*, vol. 28, no. 22, pp. 5613–5623, Oct. 2014, doi: 10.1002/hyp.10073.

[57] *Urban Hydrology for Small Watersheds*. Soil Conservation Service, Engineering Division U.S. Department of Agriculture, 1986.

[58] G. Brunner, “HEC-RAS River Analysis System- 2D Modeling User’s Manual Version 5.0,” US Army Corps of Engineers, Computer Program Documentation CPD-68A, Feb. 2016. Accessed: Apr. 21, 2021. [Online]. Available: https://www.hec.usace.army.mil/confluence/rasdocs/r2dum/latest/running-a-model-with-2d-flow-areas/computation-progress-numerical-stability-and-volume-accounting.

[59] A. Pathan and P. Agnihotri, “2-D Unsteady Flow Modelling and Inundation Mapping for Lower Region of Purna Basin Using HEC-RAS,” *Nature Environment and Pollution Technology*, vol. 19, no. 1, pp. 277–285, Mar. 2020.

[60] M. Bhandari, N. Nyaupane, S. R. Mote, A. Kalra, and S. Ahmad, “2D Unsteady Flow Routing and Flood Inundation Mapping for Lower Region of Brazos River Watershed,” pp. 292–303, May 2017, doi: 10.1061/9780784480625.027.

[61] M. Farooq, M. Shafique, and M. S. Khattak, “Flood hazard assessment and mapping of River Swat using HEC-RAS 2D model and high-resolution 12-m TanDEM-X DEM (WorldDEM),” *Nat Hazards*, vol. 97, no. 2, pp. 477–492, Jun. 2019, doi: 10.1007/s11069-019-03638-9.

[62] S. Rivera, A. Hernandez, R. Ramsey, G. Suarez, and S. Rodriguez, “Predicting flood hazard areas: A SWAT and HEC-RAS simulations conducted in aguan river basin of honduras, central America,” *Central America ASPRS 2007 Annual Conference*, May 2007.

[63] S. J. Zeiger and J. A. Hubbart, “Measuring and modeling event-based environmental flows: An assessment of HEC-RAS 2D rain-on-grid simulations,” *Journal of Environmental Management*, vol. 285, p. 112125, May 2021, doi: 10.1016/j.jenvman.2021.112125.

[64] M. Sholichin and W. Qadri, “Predicting flood hazards area using swat and hec-ras simulation in Bila river, South Sulawesi,” *IOP Conf. Ser.: Earth Environ. Sci.*, vol. 437, p. 012055, Feb. 2020, doi: 10.1088/1755-1315/437/1/012055.

[65] G. J. Arcement and V. R. Schneider, “Guide for Selecting Manning’s Roughness Coefficents for Natural Channels and Flood Plains,” U.S. Department of Transportation, Federal Highway Administration, USGS Water-Supply Paper 2339.

[66] C. Janssen, “Manning’s n Values for Various Land Covers To Use for Dam Breach Analyses by NRCS in Kansas.” Jul. 12, 2016.

[67] B. Lioi, A. Gioia, V. Totaro, G. Balacco, V. Iacobellis, and G. Chiaia, “Coupled Use of Hydrologic-Hydraulic Model and Geomorphological Descriptors for Flood-Prone Areas Evaluation: A Case Study of Lama Lamasinata,” in *Computational Science and Its Applications – ICCSA 2020*, Sep. 2020, pp. 607–619, doi: 10.1007/978-3-030-58811-3_44.

[68] S. Manfreda, M. Di Leo, and A. Sole, “Detection of Flood-Prone Areas Using Digital Elevation Models,” *Journal of Hydrologic Engineering*, vol. 16, no. 10, pp. 781–790, Jan. 2011, doi: 10.1061/(ASCE)HE.1943-5584.0000367.

[69] S. Manfreda *et al.*, “Flood-prone areas assessment using linear binary classifiers based on flood maps obtained from 1D and 2D hydraulic models,” *Nat Hazards*, vol. 79, no. 2, pp. 735–754, Jun. 2015, doi: 10.1007/s11069-015-1869-5.

[70] “Picterra – Geospatial imagery analysis made easy,” *Picterra*. https://picterra.ch/ (accessed Apr. 14, 2021).

[71] M. Kubat, R. C. Holte, and S. Matwin, “Machine Learning for the Detection of Oil Spills in Satellite Radar Images,” *Machine Learning*, vol. 30, no. 2, pp. 195–215, Feb. 1998, doi: 10.1023/A:1007452223027.

[72] P. Prasanna *et al.*, “Automated Crack Detection on Concrete Bridges,” *IEEE Transactions on Automation Science and Engineering*, vol. 13, no. 2, pp. 591–599, Apr. 2016, doi: 10.1109/TASE.2014.2354314.

[73] A. Purser, M. Bergmann, T. Lundälv, J. Ontrup, and T. W. Nattkemper, “Use of machine-learning algorithms for the automated detection of cold-water coral habitats: a pilot study,” *Marine Ecology Progress Series*, vol. 397, pp. 241–251, Dec. 2009, doi: 10.3354/meps08154.

[74] Q.-S. Xu and Y.-Z. Liang, "Monte Carlo cross validation," *Chemometrics and Intelligent Laboratory Systems*, vol. 56, no. 1, pp. 1–11, Apr. 2001, doi: 10.1016/S0169-7439(00)00122-2.

[75] "UNHCR registers over 41,000 people in congested Dzaleka Refugee Camp," *ReliefWeb*, Nov. 26, 2019. https://reliefweb.int/report/malawi/unhcr-registers-over-41000-people-congested-dzaleka-refugee-camp (accessed Feb. 12, 2021).

[76] J. A. Dijkshoorn, J. G. B. Leenaars, J. Huting, and B. Kempen, "Soil and Terrain database of the Republic of Malawi," *ISRIC-World Soil Information, Wageningen*, vol. 2016/01, p. 38, 2016.

[77] P. Schad, C. Huyssteen, and E. Micheli, "World reference base for soil resources 2014: International soil classification system for naming soils and creating legends for soil maps," Food and Agriculture Organization of the United Nations, Rome, World Soil Resources Reports 106, 2014.

[78] Y. Zhang, J. Hou, J. Gu, C. Huang, and X. Li, "SWAT-Based Hydrological Data Assimilation System (SWAT-HDAS): Description and Case Application to River Basin-Scale Hydrological Predictions," *Journal of Advances in Modeling Earth Systems*, vol. 9, no. 8, pp. 2863–2882, 2017, doi: https://doi.org/10.1002/2017MS001144.

Appendix A: Dzaleka Refugee Camp Flight Approval

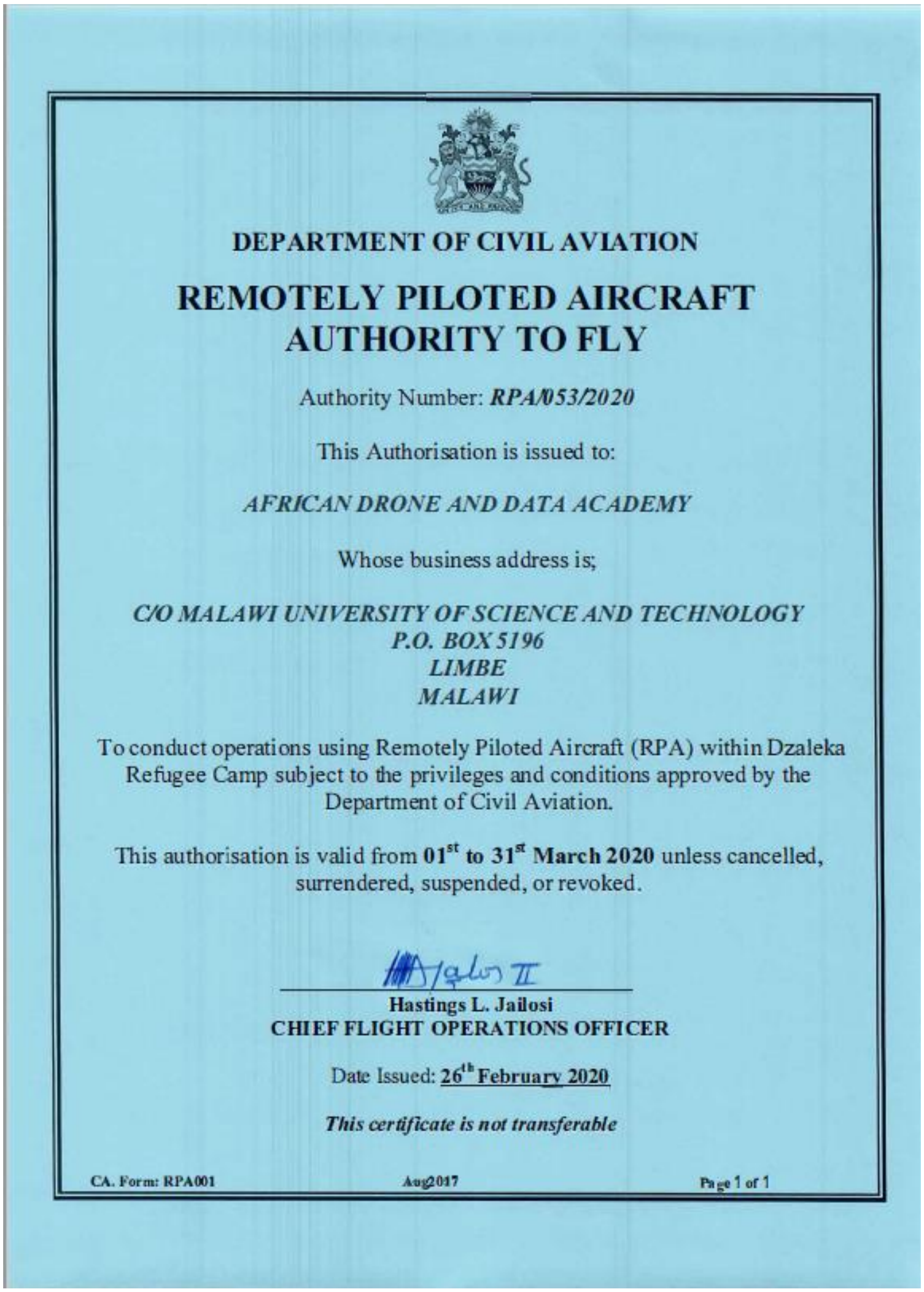

DEPARTMENT OF CIVIL AVIATION

REMOTELY PILOTED AIRCRAFT AUTHORITY TO FLY

Authority Number: ***RPA/053/2020***

This Authorisation is issued to:

AFRICAN DRONE AND DATA ACADEMY

Whose business address is;

C/O MALAWI UNIVERSITY OF SCIENCE AND TECHNOLOGY
P.O. BOX 5196
LIMBE
MALAWI

To conduct operations using Remotely Piloted Aircraft (RPA) within Dzaleka Refugee Camp subject to the privileges and conditions approved by the Department of Civil Aviation.

This authorisation is valid from **01st to 31st March 2020** unless cancelled, surrendered, suspended, or revoked.

Hastings L. Jailosi
CHIEF FLIGHT OPERATIONS OFFICER

Date Issued: **26th February 2020**

This certificate is not transferable

CA. Form: RPA001 Aug2017 Page 1 of 1

Appendix B: Pix4D Settings

Processing Options: 1. Initial Processing

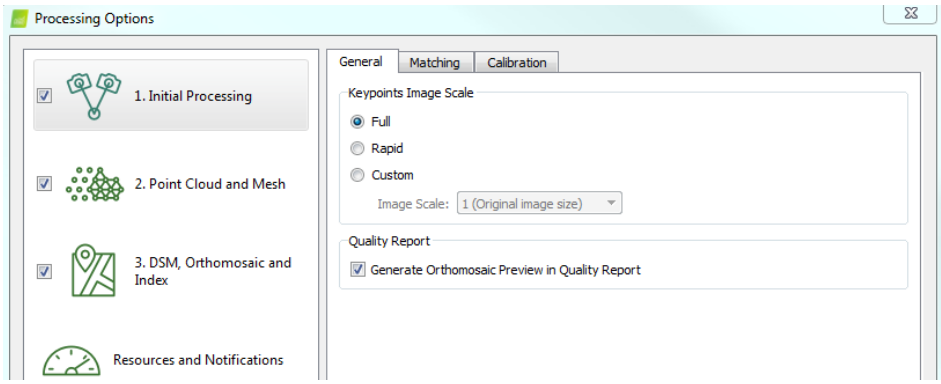

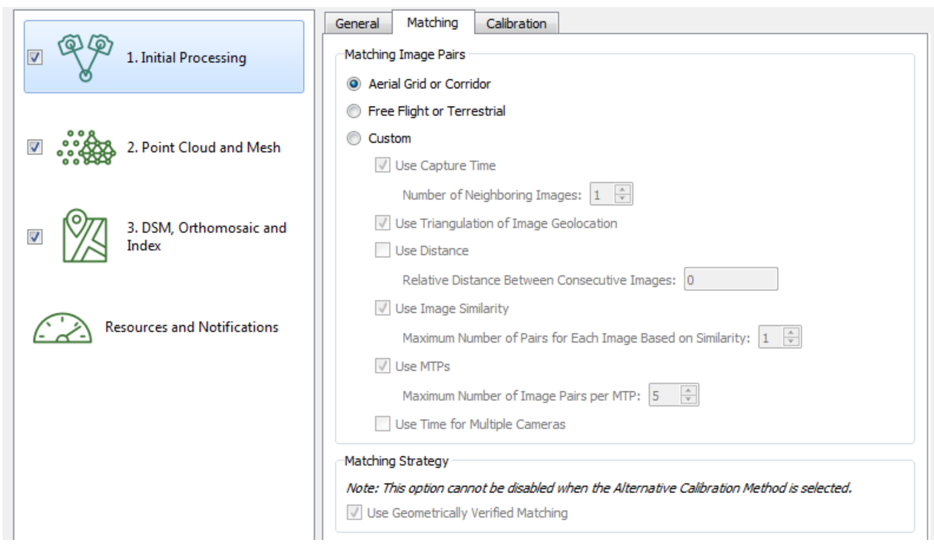

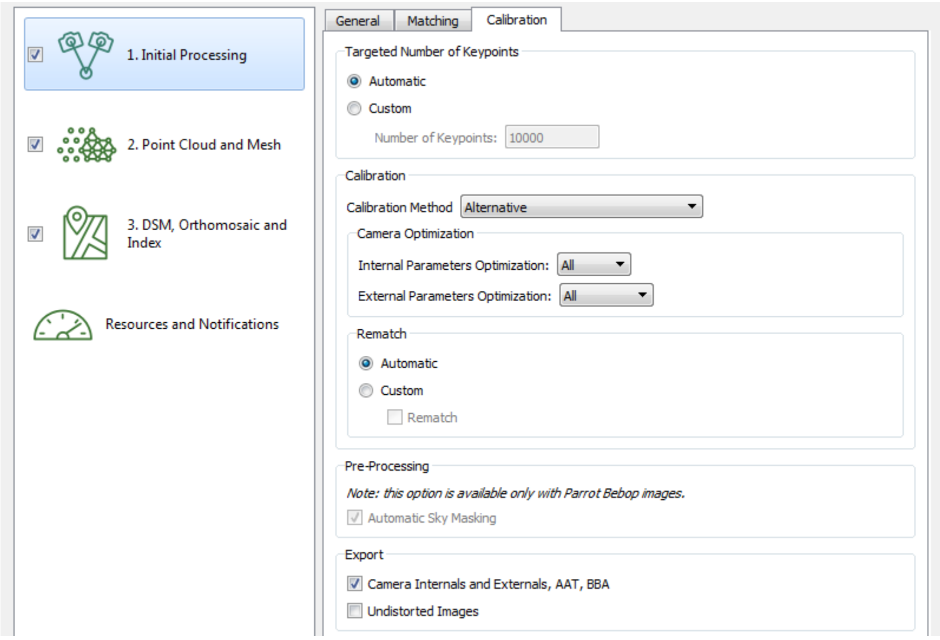

Processing Options: 2. Point Cloud and Mesh

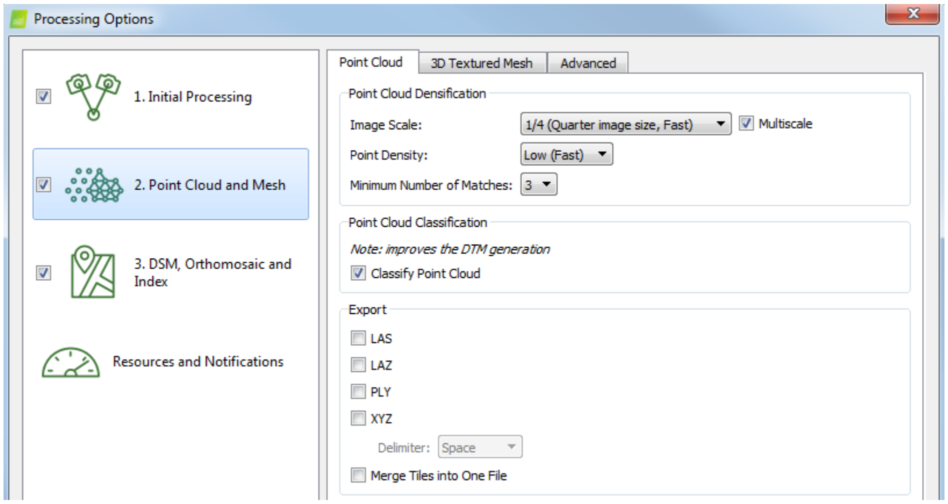

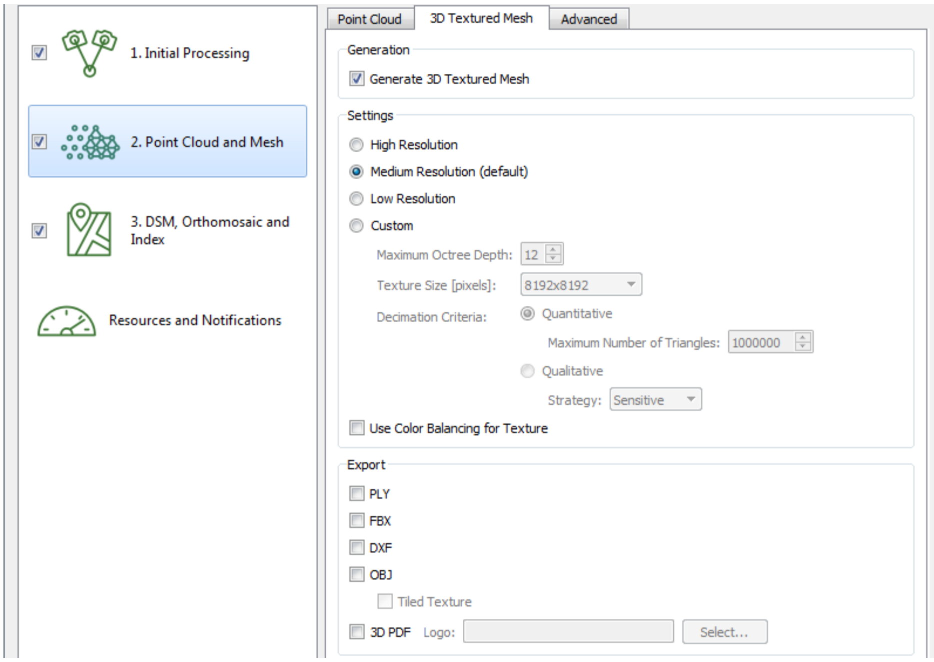
1. Initial Processing
2. Point Cloud and Mesh
3. DSM, Orthomosaic and Index
Resources and Notifications
Point Cloud
3D Textured Mesh
Advanced
Generation
Generate 3D Textured Mesh
Settings
High Resolution
Medium Resolution (default)
Low Resolution
Custom
Maximum Octree Depth: 12
Texture Size [pixels]: 8192x8192
Decimation Criteria:
Quantitative
Maximum Number of Triangles: 1000000
Qualitative
Strategy: Sensitive
Use Color Balancing for Texture
Export
PLY
FBX
DXF
OBJ
Tiled Texture
3D PDF
Logo:
Select...

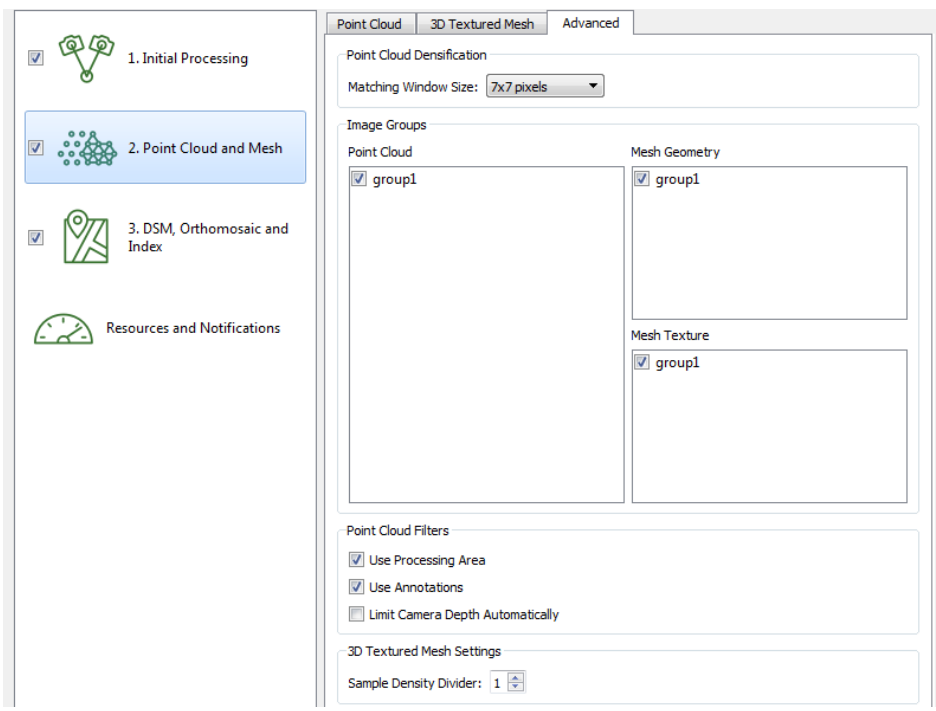
1. Initial Processing
2. Point Cloud and Mesh
3. DSM, Orthomosaic and Index
Resources and Notifications
Point Cloud
3D Textured Mesh
Advanced
Point Cloud Densification
Matching Window Size: 7x7 pixels
Image Groups
Point Cloud
group1
Mesh Geometry
group1
Mesh Texture
group1
Point Cloud Filters
Use Processing Area
Use Annotations
Limit Camera Depth Automatically
3D Textured Mesh Settings
Sample Density Divider: 1

Processing Options: 3. DSM, Orthomosaic and Index

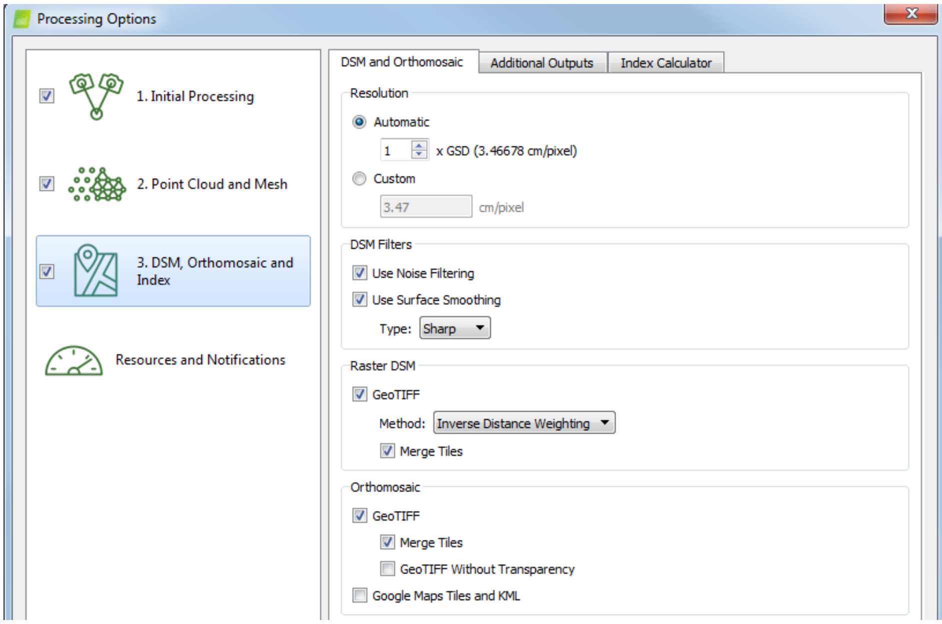

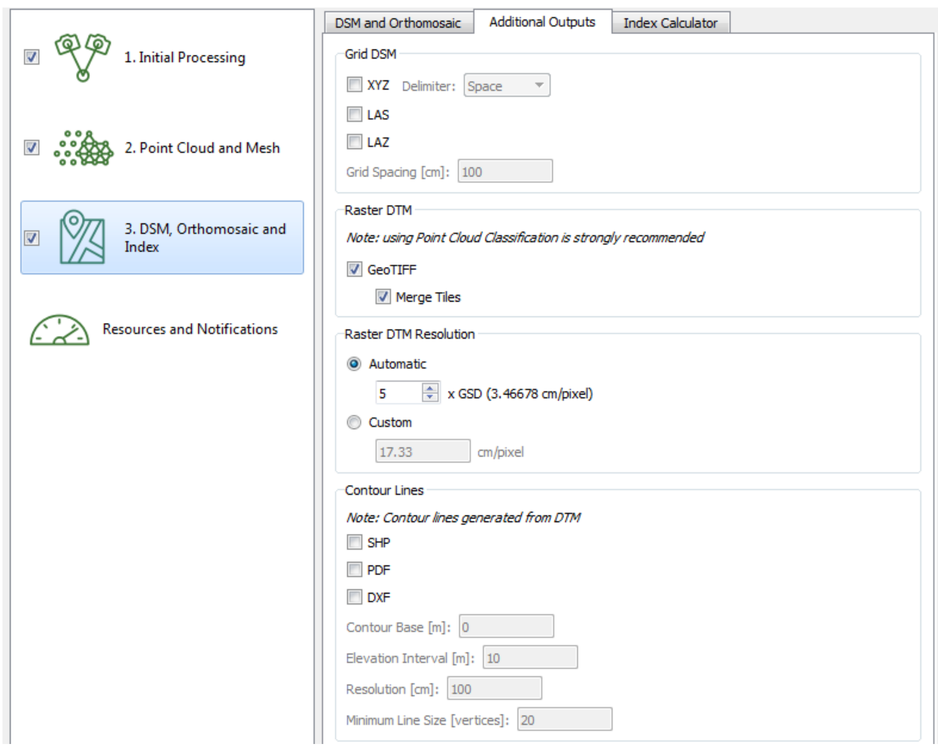

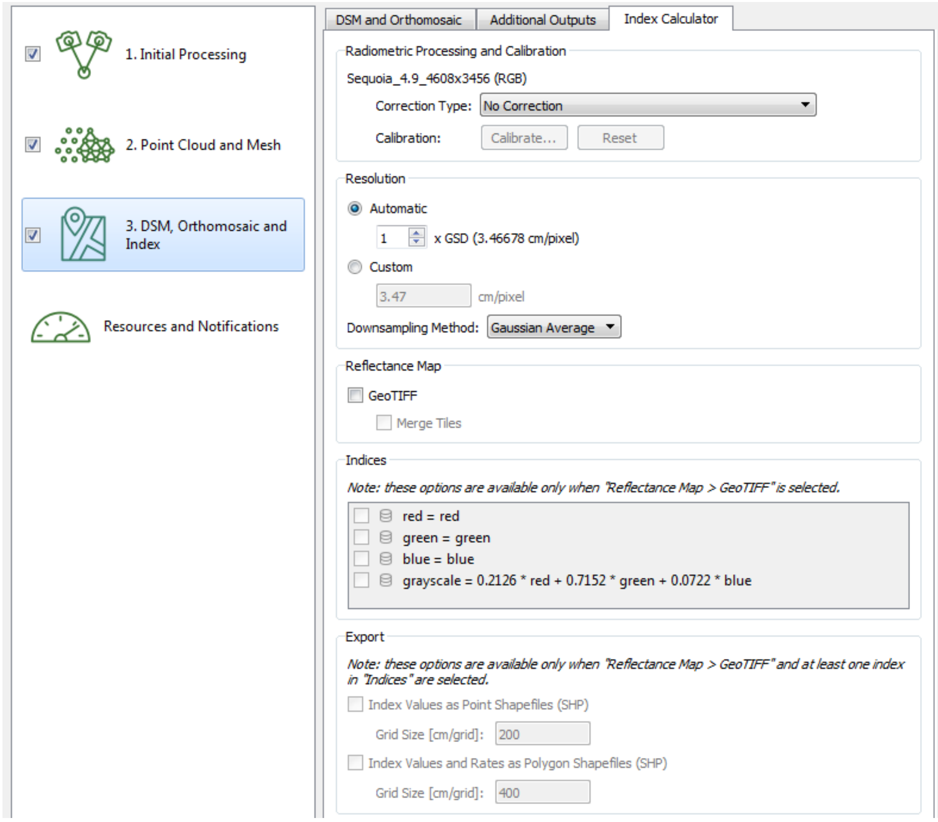

Processing Options: Resources and Notifications

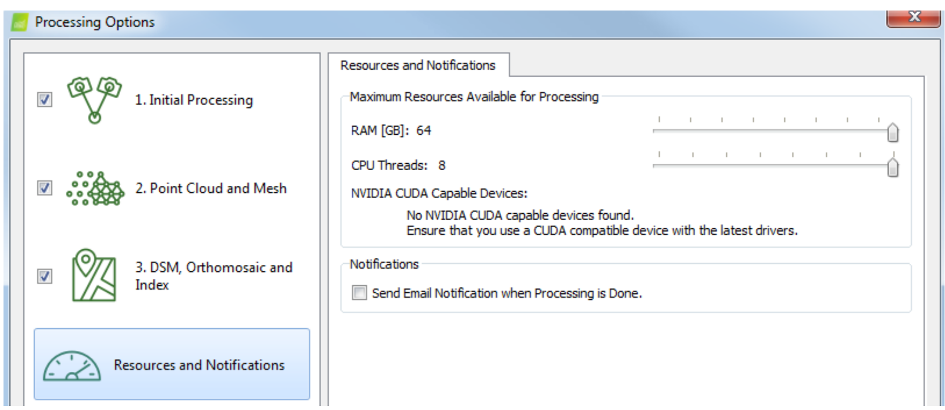

Image Properties Editor

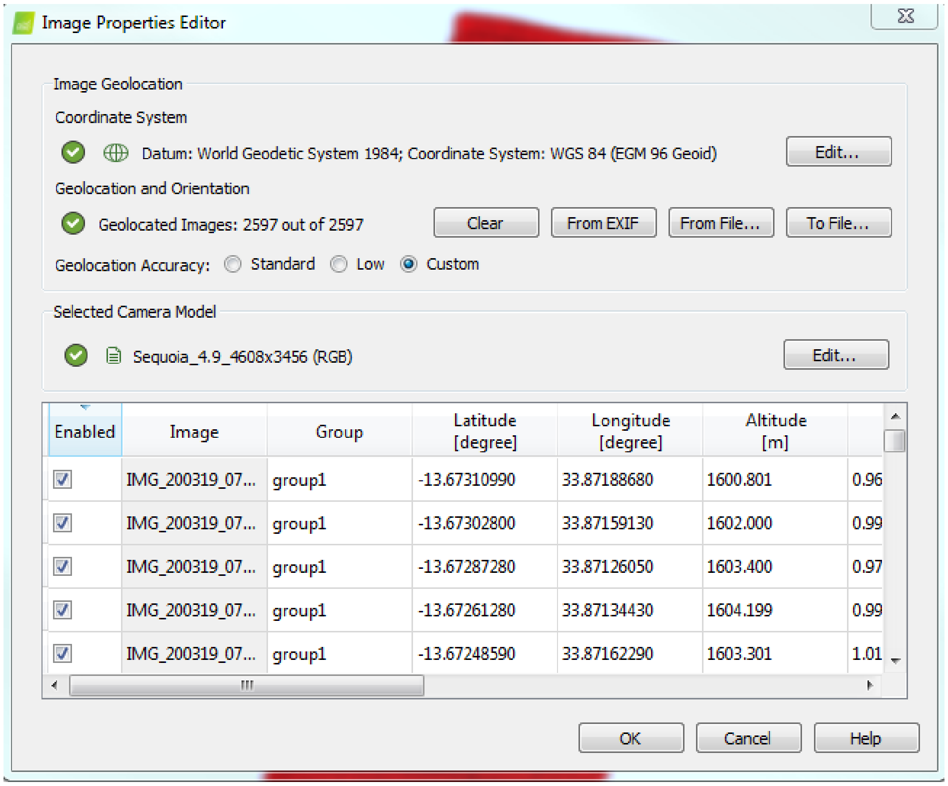

Camera Model

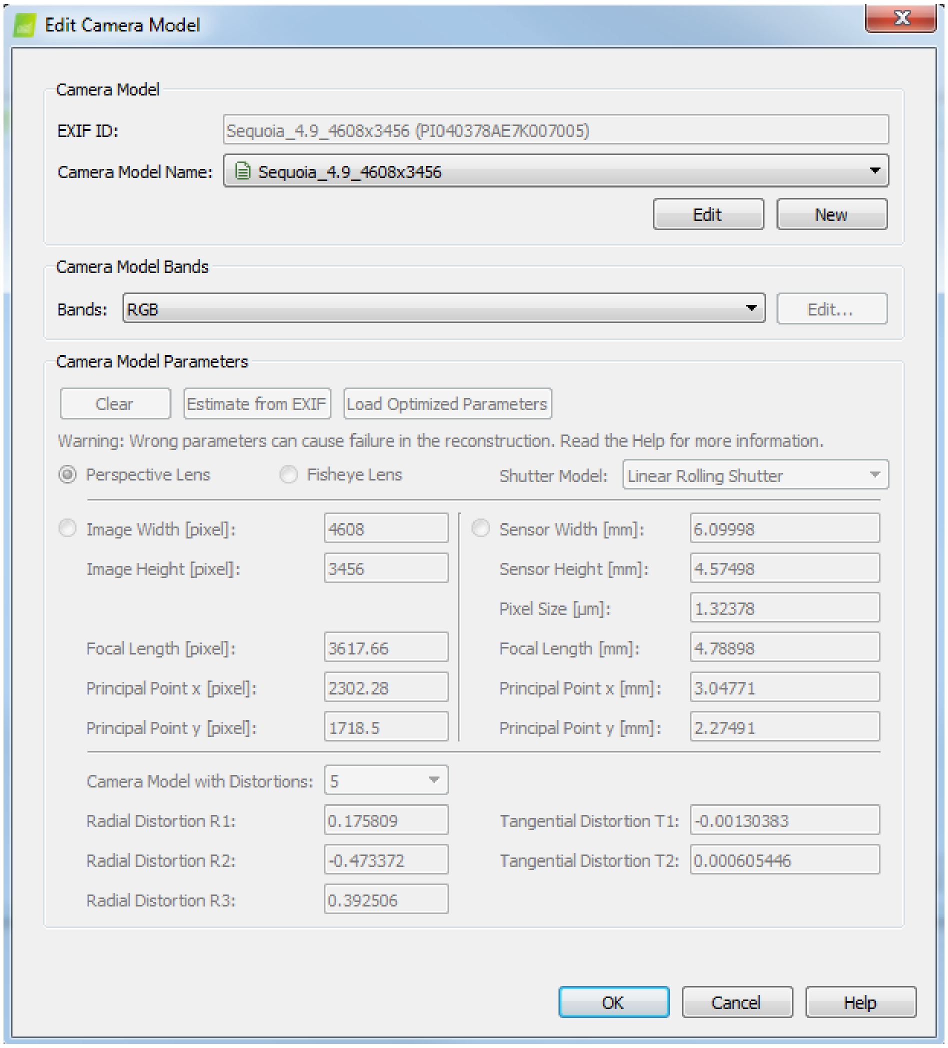

Image Coordinate System

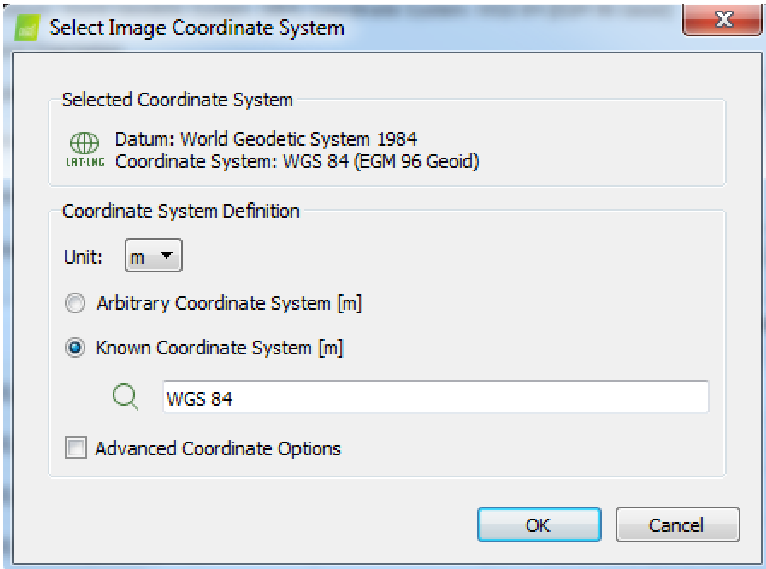

Output Coordinate System

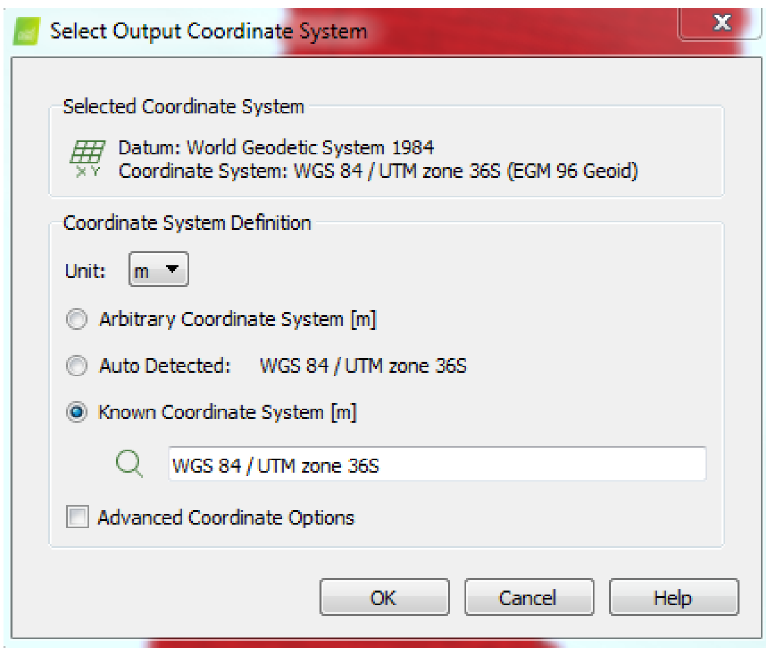

Appendix C: Collapsed Houses Ground-Truthing, Surveyors Information

Goal: Determine cause of building collapse for buildings all over Dzaleka Refugee Camp.

This research will be used by Brianna Friedman who is a master's student in the Mechanical Engineering Department at Virginia Tech, USA. Brianna is completing a flood analysis of Dzaleka Refugee Camp. She is working to support future urban planning at the camp so less houses collapse from flooding. If you have any questions or concerns please don't hesitate to email her at fbrianna@vt.edu or whatsapp her at +1-443-630-5956. She is happy to share the final report of this study with the public, if you would like a copy of the report please contact her.

This study is only interested in buildings that have collapsed from water related events (excessive rainfall/flooding). There are three main reasons that buildings at Dzaleka Refugee Camp collapse from water events:

1. Hydraulic Pressure Damage: Water running along the surface applies to much

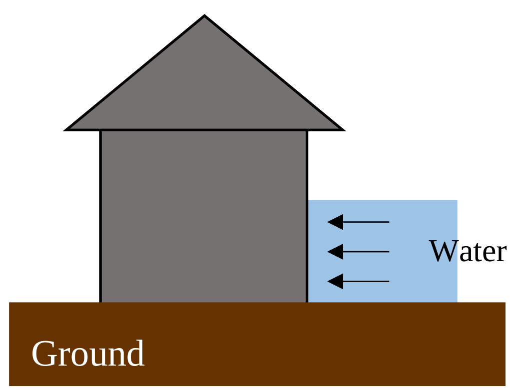

force on the walls of a building causing the walls to break or fall.

2. Foundation Undermining: Water runs along the ground so much that the ground under a building begins to erode.

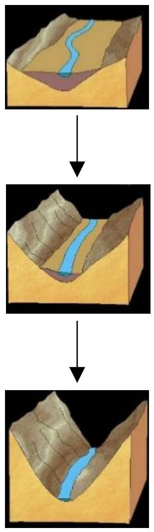

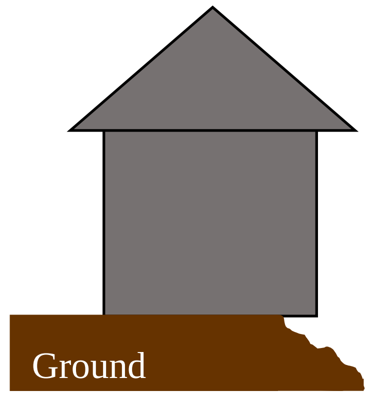

3. Roof Collapse: Rain fall applies to much force to the roof causing the roof to collapse.

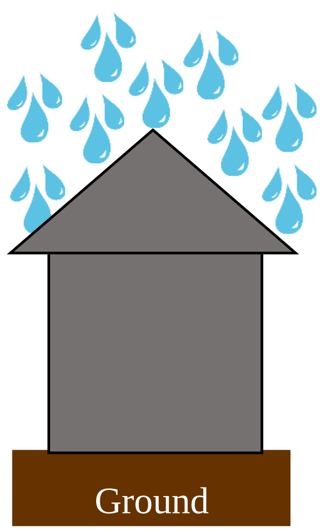

If a building has collapsed from a water related event but the reason is different than any of the ones listed above, please select "other" for reason of collapse and then type in the reason for collapse. Please include as much detail as possible.

Data collection will include:

- Location of collapsed building
- Reason for collapse (explained above)
- Photos (if possible)

Location of Data Collection: The goal is to get a representative data sample for example:

> if 10 buildings collapsed in area 1 and 20 buildings collapsed in area 2, area 2 should have about double the data points as area 1.

Appendix D: Cross-Validation Runs

	SR	WD	SR	WD	SR	WD	SR	WD	SR	WD
Foundation Undermining	0.388244	0.17027	0.732475	0.355899	0.234743	0.468171	0.611203	0.410832	0.611203	0.410832
	0.566772	0.318639	0.234743	0.468171	0.036386	0.415218	0.234743	0.468171	0.566772	0.318639
	0.036386	0.415218	0.036386	0.415218	0.611203	0.410832	0.566772	0.318639	0.388244	0.17027
	0.234743	0.468171	0.388244	0.17027	0.732475	0.355899	0.388244	0.17027	0.036386	0.415218
	0.732475	0.355899	0.611203	0.410832	0.566772	0.318639	0.732475	0.355899	0.732475	0.355899
	0.611203	0.410832	0.566772	0.318639	0.388244	0.17027	0.036386	0.415218	0.234743	0.468171
c	0.339		0.339		0.339		0.339		0.339	
Train: Count of Misclass	2		2		1		1		2	
Train: Miclass Rate	0.4		0.4		0.2		0.2		0.4	
Train: Mean	0.361262		0.376462		0.408181		0.399655		0.379206	
Test: Count of Misclass	0		0		1		1		0	
Test: Miclass Rate	0		0		1		1		0	
Test: Mean	0.478758		0.402756		0.244163		0.286794		0.398039	

	SR	WD
Foundation Undermining	0.566772	0.318639
	0.388244	0.17027
	0.234743	0.468171
	0.611203	0.410832
	0.036386	0.415218
	0.732475	0.355899
c	0.339	
Train: Count of Misclass	2	
Train: Miclass Rate	0.4	
Train: Mean	0.360302	
Test: Count of Misclass	0	
Test: Miclass Rate	0	
Test: Mean	0.483558	

	SR	WD	SR	WD	SR	WD	SR	WD	SR	WD
Hydraulic Pressure	0.035452	0.402628	0.113301	0.355736	0.065324	0.345395	0.525248	0.487621	0.113301	0.355736
	0.113301	0.355736	0.035722	0.26507	0.113301	0.355736	0.056681	0.513733	0.197712	0.511794
	0.035722	0.26507	0.41379	0	0.919594	0.348649	0.552322	0.377322	0.933236	0.278508
	0.989627	0.377271	0.989627	0.377271	0.454332	0.407579	0.137136	0.413253	0.28452	0.490333
	0.137298	0.41976	0.552322	0.377322	0.525248	0.487621	0.05329	0.351236	0.41379	0
	0.552322	0.377322	0.208577	0.599381	0.531233	0.522227	0.061322	0.388267	0.036544	0.356977
	0.501258	0.319729	0.137298	0.41976	0.035452	0.402628	0.531233	0.522227	0.776816	0.474498
	0.531233	0.522227	0.776816	0.474498	0.28452	0.490333	0.41379	0	0.065324	0.345395
	0.036544	0.356977	0.454332	0.407579	0.137136	0.413253	0.776816	0.474498	0.552322	0.377322
	0.065589	0.541973	0.531233	0.522227	0.497546	0.367607	0.129893	0.409741	0.454332	0.407579
	0.538636	0.553882	0.065589	0.541973	0.93702	0.098066	0.065589	0.541973	0.208577	0.599381
	0.197712	0.511794	0.538636	0.553882	0.538636	0.553882	0.036544	0.356977	0.497546	0.367607
	0.208577	0.599381	0.919594	0.348649	0.41379	0	0.497546	0.367607	0.93702	0.098066
	0.137136	0.413253	0.933236	0.278508	0.035722	0.26507	0.93702	0.098066	0.919594	0.348649
	0.129893	0.409741	0.137136	0.413253	0.056681	0.513733	0.137298	0.41976	0.531233	0.522227
	0.93702	0.098066	0.061322	0.388267	0.552322	0.377322	0.538636	0.553882	0.989627	0.377271
	0.056681	0.513733	0.501258	0.319729	0.129893	0.409741	0.989627	0.377271	0.035722	0.26507
	0.41379	0	0.065324	0.345395	0.137298	0.41976	0.113301	0.355736	0.137298	0.41976
	0.933236	0.278508	0.056681	0.513733	0.989627	0.377271	0.919594	0.348649	0.035452	0.402628
	0.065324	0.345395	0.036544	0.356977	0.208577	0.599381	0.035452	0.402628	0.061322	0.388267
	0.454332	0.407579	0.93702	0.098066	0.776816	0.474498	0.454332	0.407579	0.525248	0.487621
	0.919594	0.348649	0.497546	0.367607	0.065589	0.541973	0.28452	0.490333	0.538636	0.553882
	0.28452	0.490333	0.28452	0.490333	0.036544	0.356977	0.933236	0.278508	0.05329	0.351236
	0.525248	0.487621	0.035452	0.402628	0.197712	0.511794	0.208577	0.599381	0.501258	0.319729
	0.061322	0.388267	0.129893	0.409741	0.061322	0.388267	0.197712	0.511794	0.065589	0.541973
	0.776816	0.474498	0.197712	0.511794	0.933236	0.278508	0.035722	0.26507	0.056681	0.513733
	0.497546	0.367607	0.05329	0.351236	0.05329	0.351236	0.501258	0.319729	0.137136	0.413253
	0.05329	0.351236	0.525248	0.487621	0.501258	0.319729	0.065324	0.345395	0.129893	0.409741
c	0.071		0.074		0.071		0.071		0.39	
Train: Count of Misclass	9		10		7		8		8	
Train: Miclass Rate	0.409091		0.454545		0.318182		0.363636		0.363636	
Train: Mean	0.381284		0.38055		0.397533		0.392235		0.397593	
Test: Count of Misclass	3		2		5		4		5	

Test: Miclass Rate	0.5		0.333333		0.833333		0.666667		0.833333	
Test: Mean	0.422324		0.424623		0.362745		0.382173		0.320566	

	SR	WD	SR	WD	SR	WD	SR	WD	SR	WD
Hydraulic Pressure	0.41379	0	0.531233	0.522227	0.531233	0.522227	0.035722	0.26507	0.525248	0.487621
	0.933236	0.278508	0.036544	0.356977	0.525248	0.487621	0.05329	0.351236	0.065324	0.345395
	0.035452	0.402628	0.919594	0.348649	0.208577	0.599381	0.035452	0.402628	0.989627	0.377271
	0.208577	0.599381	0.525248	0.487621	0.035452	0.402628	0.501258	0.319729	0.538636	0.553882
	0.035722	0.26507	0.497546	0.367607	0.41379	0	0.056681	0.513733	0.061322	0.388267
	0.552322	0.377322	0.05329	0.351236	0.538636	0.553882	0.061322	0.388267	0.28452	0.490333
	0.989627	0.377271	0.137298	0.41976	0.137298	0.41976	0.129893	0.409741	0.129893	0.409741
	0.065589	0.541973	0.137136	0.413253	0.933236	0.278508	0.525248	0.487621	0.552322	0.377322
	0.776816	0.474498	0.113301	0.355736	0.776816	0.474498	0.989627	0.377271	0.501258	0.319729
	0.525248	0.487621	0.93702	0.098066	0.061322	0.388267	0.538636	0.553882	0.93702	0.098066
	0.501258	0.319729	0.28452	0.490333	0.035722	0.26507	0.137298	0.41976	0.137298	0.41976
	0.056681	0.513733	0.035452	0.402628	0.197712	0.511794	0.036544	0.356977	0.208577	0.599381
	0.919594	0.348649	0.035722	0.26507	0.28452	0.490333	0.197712	0.511794	0.531233	0.522227
	0.137298	0.41976	0.552322	0.377322	0.065324	0.345395	0.776816	0.474498	0.197712	0.511794
	0.538636	0.553882	0.065589	0.541973	0.05329	0.351236	0.28452	0.490333	0.497546	0.367607
	0.197712	0.511794	0.776816	0.474498	0.552322	0.377322	0.454332	0.407579	0.035452	0.402628
	0.454332	0.407579	0.065324	0.345395	0.919594	0.348649	0.137136	0.413253	0.933236	0.278508
	0.036544	0.356977	0.41379	0	0.129893	0.409741	0.208577	0.599381	0.056681	0.513733
	0.065324	0.345395	0.933236	0.278508	0.501258	0.319729	0.531233	0.522227	0.776816	0.474498
	0.05329	0.351236	0.061322	0.388267	0.137136	0.413253	0.113301	0.355736	0.41379	0
	0.129893	0.409741	0.989627	0.377271	0.065589	0.541973	0.065589	0.541973	0.065589	0.541973
	0.531233	0.522227	0.197712	0.511794	0.056681	0.513733	0.065324	0.345395	0.454332	0.407579
	0.93702	0.098066	0.129893	0.409741	0.454332	0.407579	0.41379	0	0.137136	0.413253
	0.113301	0.355736	0.056681	0.513733	0.497546	0.367607	0.93702	0.098066	0.05329	0.351236
	0.497546	0.367607	0.538636	0.553882	0.113301	0.355736	0.552322	0.377322	0.036544	0.356977
	0.137136	0.413253	0.208577	0.599381	0.989627	0.377271	0.497546	0.367607	0.919594	0.348649
	0.061322	0.388267	0.454332	0.407579	0.93702	0.098066	0.919594	0.348649	0.113301	0.355736
	0.28452	0.490333	0.501258	0.319729	0.036544	0.356977	0.933236	0.278508	0.035722	0.26507
c	0.071		0.074		0.071		0.02		0.074	
Train: Count of Misclass	8		11		8		7		8	
Train: Miclass Rate	0.363636		0.5		0.363636		0.318182		0.363636	
Train: Mean	0.400672		0.371976		0.403788		0.428938		0.403989	
Test: Count of Misclass	4		1		4		6		4	

Test: Miclass Rate	0.666667		0.166667		0.666667		1		0.666667		
Test: Mean	0.351235		0.45606		0.33981		0.254303		0.338678		

	SR	WD	SR	WD	SR	WD	SR	WD	SR	WD
Hydraulic Pressure	0.933236	0.278508	0.525248	0.487621	0.933236	0.278508	0.552322	0.377322	0.93702	0.098066
	0.41379	0	0.129893	0.409741	0.454332	0.407579	0.28452	0.490333	0.41379	0
	0.137298	0.41976	0.035722	0.26507	0.197712	0.511794	0.989627	0.377271	0.919594	0.348649
	0.113301	0.355736	0.065324	0.345395	0.525248	0.487621	0.501258	0.319729	0.208577	0.599381
	0.525248	0.487621	0.035452	0.402628	0.137298	0.41976	0.197712	0.511794	0.531233	0.522227
	0.056681	0.513733	0.056681	0.513733	0.056681	0.513733	0.531233	0.522227	0.552322	0.377322
	0.065589	0.541973	0.501258	0.319729	0.137136	0.413253	0.113301	0.355736	0.497546	0.367607
	0.05329	0.351236	0.552322	0.377322	0.113301	0.355736	0.129893	0.409741	0.137298	0.41976
	0.035722	0.26507	0.137136	0.413253	0.036544	0.356977	0.525248	0.487621	0.065589	0.541973
	0.035452	0.402628	0.919594	0.348649	0.208577	0.599381	0.065324	0.345395	0.113301	0.355736
	0.061322	0.388267	0.197712	0.511794	0.05329	0.351236	0.035452	0.402628	0.197712	0.511794
	0.454332	0.407579	0.208577	0.599381	0.531233	0.522227	0.93702	0.098066	0.538636	0.553882
	0.989627	0.377271	0.989627	0.377271	0.93702	0.098066	0.065589	0.541973	0.061322	0.388267
	0.552322	0.377322	0.41379	0	0.065324	0.345395	0.538636	0.553882	0.035452	0.402628
	0.129893	0.409741	0.061322	0.388267	0.989627	0.377271	0.035722	0.26507	0.454332	0.407579
	0.065324	0.345395	0.933236	0.278508	0.538636	0.553882	0.41379	0	0.056681	0.513733
	0.036544	0.356977	0.454332	0.407579	0.552322	0.377322	0.056681	0.513733	0.05329	0.351236
	0.208577	0.599381	0.137298	0.41976	0.129893	0.409741	0.137298	0.41976	0.28452	0.490333
	0.531233	0.522227	0.497546	0.367607	0.776816	0.474498	0.061322	0.388267	0.035722	0.26507
	0.137136	0.413253	0.28452	0.490333	0.919594	0.348649	0.933236	0.278508	0.501258	0.319729
	0.919594	0.348649	0.05329	0.351236	0.035452	0.402628	0.036544	0.356977	0.989627	0.377271
	0.197712	0.511794	0.113301	0.355736	0.501258	0.319729	0.919594	0.348649	0.036544	0.356977
	0.501258	0.319729	0.036544	0.356977	0.497546	0.367607	0.497546	0.367607	0.525248	0.487621
	0.776816	0.474498	0.776816	0.474498	0.41379	0	0.137136	0.413253	0.933236	0.278508
	0.28452	0.490333	0.531233	0.522227	0.065589	0.541973	0.454332	0.407579	0.129893	0.409741
	0.538636	0.553882	0.93702	0.098066	0.035722	0.26507	0.208577	0.599381	0.776816	0.474498
	0.497546	0.367607	0.065589	0.541973	0.061322	0.388267	0.776816	0.474498	0.137136	0.413253
	0.93702	0.098066	0.538636	0.553882	0.28452	0.490333	0.05329	0.351236	0.065324	0.345395
c	0.071		0.071		0.071		0.071		0.071	
Train: Count of Misclass	9		10		8		10		10	
Train: Miclass Rate	0.409091		0.454545		0.363636		0.454545		0.454545	
Train: Mean	0.387756		0.379571		0.405376		0.379234		0.386451	
Test: Count of Misclass	3		2		4		2		2	

Test: Miclass Rate	0.5		0.333333		0.666667		0.333333		0.333333	
Test: Mean	0.398594		0.428606		0.333987		0.429843		0.40338	